1 OF 1
AD
A058 397
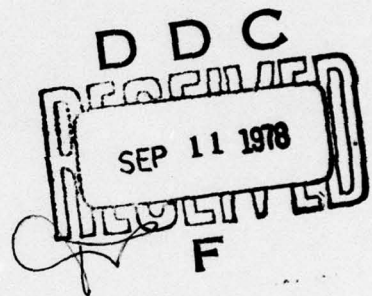
END
DATE
FILMED
-11-78
DDC

LEVEL

ATMOSPHERIC LIQUID WATER AND RAINFALL RATE DETERMINATION

OVER LAND SURFACES USING THE NIMBUS VI

SCANNING MICROWAVE SPECTROMETER

by

Alan Douglas Duff

A thesis submitted to the faculty of The
University of Utah in partial fulfillment of the requirements
for the degree of

Master of Science

Department of Meteorology

University of Utah

March 1978

REPORT DOCUMENTATION PAGE	READ INSTRUCTIONS BEFORE COMPLETING FORM

1. REPORT NUMBER AFIT-CI-78-61	2. GOVT ACCESSION NO.	3. RECIPIENT'S CATALOG NUMBER
4. TITLE (and Subtitle) Atmospheric Liquid Water and Rainfall Rate Determination Over Land Surfaces Using The Nimbus VI Scanning Microwave Spectrometer.		5. TYPE OF REPORT & PERIOD COVERED Master's Thesis
		6. PERFORMING ORG. REPORT NUMBER
7. AUTHOR(s) Alan Douglas Duff		8. CONTRACT OR GRANT NUMBER(s)
9. PERFORMING ORGANIZATION NAME AND ADDRESS AFIT Student at the University of Utah, Salt Lake City, UT		10. PROGRAM ELEMENT, PROJECT, TASK AREA & WORK UNIT NUMBERS
11. CONTROLLING OFFICE NAME AND ADDRESS AFIT/CI WPAFB OH 45433		12. REPORT DATE 11 MAR 1978
		13. NUMBER OF PAGES 61 Pages 72 p.
14. MONITORING AGENCY NAME & ADDRESS(if different from Controlling Office)		15. SECURITY CLASS. (of this report) Unclassified
		15a. DECLASSIFICATION/DOWNGRADING SCHEDULE

16. DISTRIBUTION STATEMENT (of this Report)

Approved for Public Release; Distribution Unlimited

17. DISTRIBUTION STATEMENT (of the abstract entered in Block 20, if different from Report)

18. SUPPLEMENTARY NOTES

JOSEPH P. HIPPS, Major, USAF
Director of Information, AFIT

AUG 15 1978

19. KEY WORDS (Continue on reverse side if necessary and identify by block number)

20. ABSTRACT (Continue on reverse side if necessary and identify by block number)

012 200

78 08 31 014

DD FORM 1473 1 JAN 73   EDITION OF 1 NOV 65 IS OBSOLETE

ATMOSPHERIC LIQUID WATER AND RAINFALL RATE DETERMINATION

OVER LAND SURFACES USING THE NIMBUS VI

SCANNING MICROWAVE SPECTROMETER

by

Alan Douglas Duff

An abstract of a thesis submitted to the faculty of The
University of Utah in partial fulfillment of the requirements
for the degree of

Master of Science

Kuo-Nan Liou   Chairman, Supervisory Committee

Department of Meteorology

Department of Meteorology

The University of Utah

March 1978
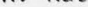
THE UNIVERSITY OF UTAH GRADUATE SCHOOL

SUPERVISORY COMMITTEE APPROVAL

of a thesis submitted by

Alan Douglas Duff

I have read this thesis and have found it to be of satisfactory quality for a master's degree.

March 10, 1978
Date

Kuo-Nan Liou

Chairman, Supervisory Committee

I have read this thesis and have found it to be of satisfactory quality for a master's degree.

March 10, 1978
Date

S. K. Kao

Member, Supervisory Committee

I have read this thesis and have found it to be of satisfactory quality for a master's degree.

March 13, 1978
Date

E. G. Astling

Member, Supervisory Committee

THE UNIVERSITY OF UTAH GRADUATE SCHOOL

FINAL READING APPROVAL

To the Graduate Council of The University of Utah:

I have read the thesis of ___Alan Douglas Duff___ in its final form and have found that (1) its format, citations, and bibliographic style are consistent and acceptable; (2) its illustrative materials including figures, tables, and charts are in place; and (3) the final manuscript is satisfactory to the Supervisory Committee and is ready for submission to the Graduate School.

March 10, 1978
Date

Kuo-Nan Liou
Member, Supervisory Committee

Approved for the Major Department

S. K. Kao
Chairman/Dean

Approved for the Graduate Council

Sterling M. McMurrin
Dean of The Graduate School

04
6-76

ABSTRACT

The purpose of this study is to determine water vapor and liquid water content from the Nimbus 6 SCAMS instrument over land surfaces. The radiative properties of clouds and precipitation in the SCAMS channels are investigated using the discrete-ordinate method for approximating the solution of the radiative transfer as it is applied to non-isothermal, inhomogeneous cloudy atmospheres. An examination of the problem of variations in surface emissivity over land in the microwave spectrum is included. Analysis of the upwelling radiances from the model in the presence of clouds indicates that the concentration of water vapor and liquid water in atmospheres over land surfaces has a consistent and predictable effect on the observed brightness temperatures.

The results of the theoretical calculations are parameterized and an empirical method to derive water vapor and liquid water from the observed upwelling radiances is described. Satellite passes from five days over the United States are used to test the empirical parameterizations of the theoretical results. The empirically derived liquid water contents for two days are compared with synoptic discussions and NOAA 4 satellite mosaics, as well as previous infrared research for the same time period (Feddes and Liou, 1978). Examples of application of this technique to global mapping of liquid water content are displayed. The use of this technique combined with infrared parameterizations to obtain accurate, global scale mapping of atmospheric moisture is discussed.

iv

ACKNOWLEDGMENTS

TABLE OF CONTENTS

Page

LIST OF FIGURES

CHAPTER 1

INTRODUCTION

One of the newest sources of meteorological data is the passive microwave spectrometer aboard the Nimbus 6. The Scanning Microwave Spectrometer (SCAMS) aboard the satellite was designed to produce global maps of tropospheric temperature profiles and liquid water and water vapor amounts over ocean surfaces. It is the effect of clouds and precipitation on the five SCAMS channels which will be addressed in this study, with particular attention to the retrieval of water vapor concentrations and liquid water content over land surfaces.

The use of passive microwave sensing from satellites to observe atmospheric water vapor and liquid water over the oceans has been well studied (see, e.g., Staelin, et al., 1976; Waters, et al., 1976 and Wilheit, et al., 1977). In these studies, however, the techniques have been based on the low emissivity of the ocean surface at microwave wavelengths and therefore on the characteristic warmness of atmospheric water vapor and liquid water against the cool background of the ocean surface. This technique becomes much more difficult to apply when the surface under the satellite scan is a solid surface, such as land or heavy vegetation. In this instance, the land brightness approaches the same temperature as the atmospheric water, the effects of which become less obvious. For this reason, the technique has not been applied over the land masses.

The nonapplicability of this technique over land surfaces has resulted in a serious gap in the global mapping mentioned earlier. This global mapping is vital to a more complete understanding of the processes of precipitation and drought. As Wilheit, et al., (1977) emphasizes, point measurements of rainfall may not accurately represent what can be the very discontinuous process of precipitation. In addition, if sensing in the microwave spectrum is to be accurately utilized, the effects of clouds on the observations must be more thoroughly understood.

The purpose of the research described here is to analytically determine the effect of clouds and precipitation on the upwelling radiance observed by the SCAMS radiometer aboard the Nimbus 6.

Chapter 2 contains a description of the physical model used in the radiative transfer program and a description of the SCAMS channel characteristics. Chapter 3 includes a section on microwave radiative transfer in a scattering atmosphere, the development of the theoretical boundary conditions for the transfer equation, and a discussion of the problems involved in determining emissivity values over land surfaces.

Chapter 4 describes the results obtained from the theoretical transfer program and the verification process used to confirm the accuracy of the computer model. Included are sections on data selection, radiative transfer in a clear atmosphere, sensitivity analyses, and radiative transfer in cloudy or precipitating conditions.

Chapter 5 contains the development of empirical formulas for the derivation of water vapor and liquid water content over land surfaces. Two examples of their use are given, and comparisons with radiosonde

observations and previous research are made.

Chapter 6 lists the conclusions of this research. Recommendations for additional research, possible applications, and limitations are listed.

CHAPTER 2

CHARACTERISTICS OF SCAMS CHANNELS AND ATMOSPHERIC MODEL

2.1 Characteristics of SCAMS Channels

The Nimbus 6 satellite is in a 1100 kilometer, sun-synchronous
polar orbit, with a local noon (ascending) and midnight (descending)
equator crossing, and an 81 degree retrograde inclination. The or-
bital period is approximately 107 minutes. The SCAMS radiometer
scans to each side of the subpoint track and provides nearly full
earth coverage every 12 hours.

The SCAMS has five channels, each centered on a different fre-
quency. The spectral characteristics of the five microwave channels
are presented in Table 1. The first channel is centered at 22.235 GHz,
located on a weak water vapor resonance. Channel 2, centered at
31.400 GHZ, is located in a spectral window, where the atmosphere is
essentially transparent at microwave frequencies. Channels 3, 4 and 5
are on the edge of an oxygen absorption band. The atmosphere is
nearly opaque at these frequencies, with peak weighting functions cen-
tered at approximately 4, 9 and 14 km, respectively, as shown in Fig-
ure 1. Channel 3 is the most useful of the three oxygen band channels
for the purpose of sensing low and middle clouds, as channels 4 and 5
peak well above most atmospheric liquid water.

The SCAMS radiometer scans the surface every sixteen seconds,
taking 13 data samples, each separated by 7.2 degrees of scan angle,
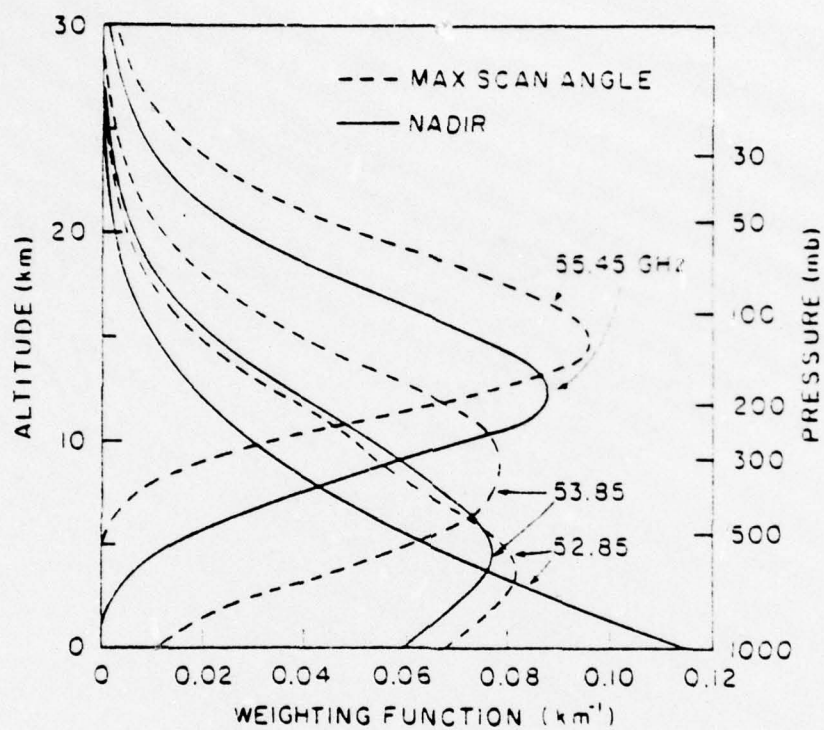
Figure 1. SCAMS weighting functions, including a component which is reflected from the surface. Source: The Nimbus 6 User's Guide.

Table 1. SCAMS Channel Characteristics

Characteristic	Channel				
	1	2	3	4	5
Frequency (GHz)	22.235	31.400	52.850	53.850	55.450
Integration Time (ms)	950	950	950	950	950
Absolute Accuracy (^{O}Krms) Long Term	2.0	2.0	2.0	2.0	2.0
Antenna Beam Width (deg)	7.5	7.5	7.5	7.5	7.5
Dynamic Range (^{O}K)	0-350	0-350	0-350	0-350	0-350

After Staelin et al. (1975).

extending between 43.2 degrees left of nadir to 43.2 degrees right of
nadir. Each sample plus step requires one second, with three seconds
at the end of each earth scan reserved for reflector rotation and
calibration using a space view and an instrument black body source.
As shown in Figure 2, the ground resolution is approximately 145 km at
nadir and 330 km at 43 degrees from nadir.

2.2 Atmospheric Model and Scattering Parameters

This study uses a plane-parallel model of the atmosphere similar
to the one described by Liou (1974a), to explore the effects of cirrus
and of low clouds, both precipitating and nonprecipitating, on the
microwave spectrum channels viewed by the SCAMS radiometer aboard
Nimbus 6, including the 60 GHz oxygen band, the 22.23 GHz water vapor
line, and the window region at 31.65 GHz. The temperature, pressure,
and water vapor profiles were taken from two sources. First, whenever
possible for verification of observed satellite data, radiosonde data
from representative ground stations was utilized. For upper
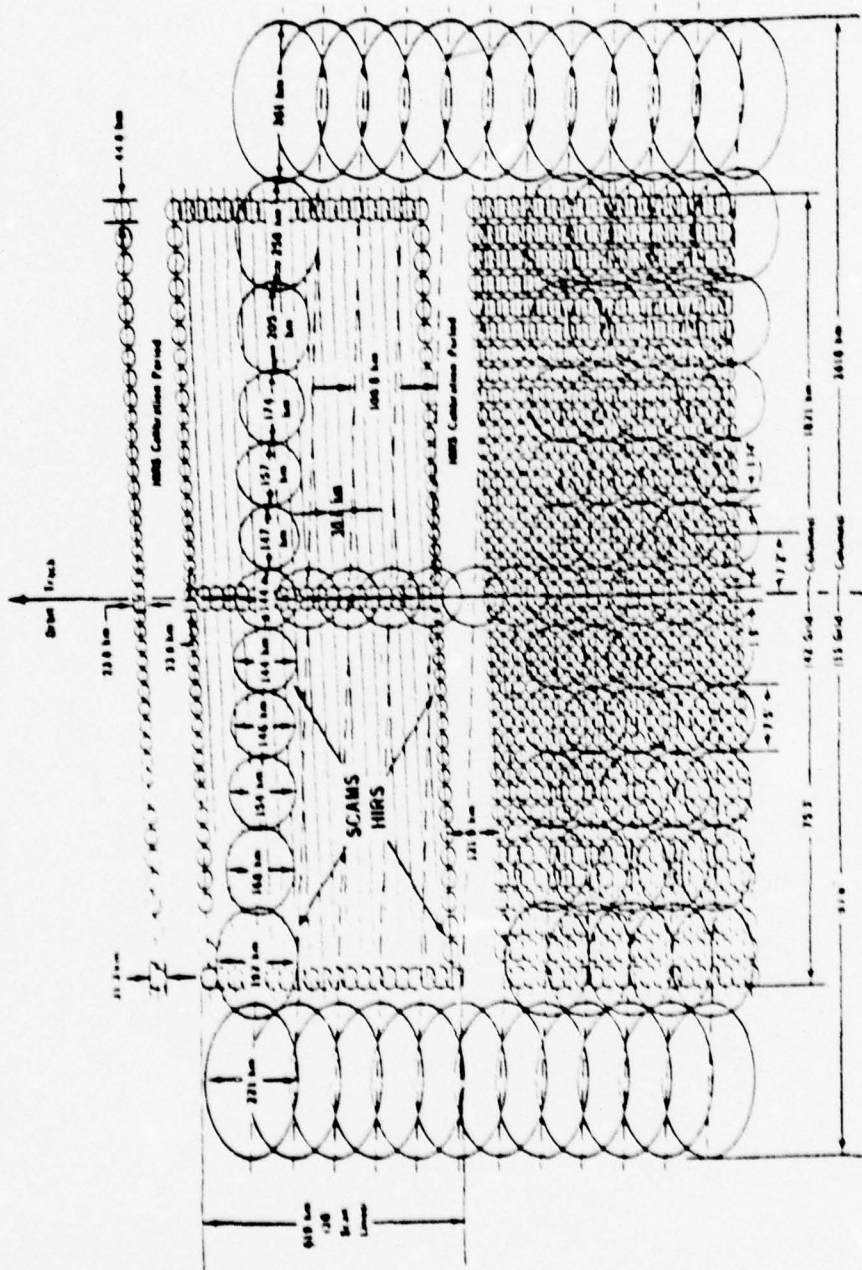
Figure 2. Scan grid patterns for HIRS and SCAMS. Source: The Nimbus 6 User's Guide.

atmospheric data and for data sparse areas, climatological tables from the 1962 Standard Atmosphere for mid-latitude summer conditions were used, as shown in Figure 3. Transmission functions and emission from water vapor and oxygen were obtained using these soundings. Figure 4 illustrates the atmosphere divided into three layers, with the cloud or precipitation layer further divided into three isothermal sublayers with each sublayer temperature assumed to be that of the observed or predicted atmosphere at that height.

The base of the cloud and the thickness of the cloud were varied to test the effect of different cloud types and amounts on microwave propagation. For nonprecipitating (water) low and middle clouds, several drop size distributions were used. First, a drop size distribution developed by Feddes and Smith (1974) was tested. Then, to determine the sensitivity of the scattering parameters to drop size distributions, a model by Deirmendjian (1969) was compared. No significant change in scattering parameters occurred between the two models. The Deirmendjian model parameters were used for all subsequent nonprecipitating cloud cases. This model is based on the equation

$$n(r) = ar^{\alpha} \exp(-br^{\gamma}) \tag{1}$$

which vanishes at $r = 0, \infty$. This distribution is called the modified gamma distribution and, by varying the constants, can be made to represent a variety of cloud types. For the cloud model used here, $a = 4.9757 \times 10^{7}$, $\alpha = 2$, $b = 15.1186$, and $\gamma = .5$.

For precipitating low clouds, a theoretical drop size distribution based on rainfall rate, first developed by Marshall and Palmer (1948), was used. The distribution is expressed by
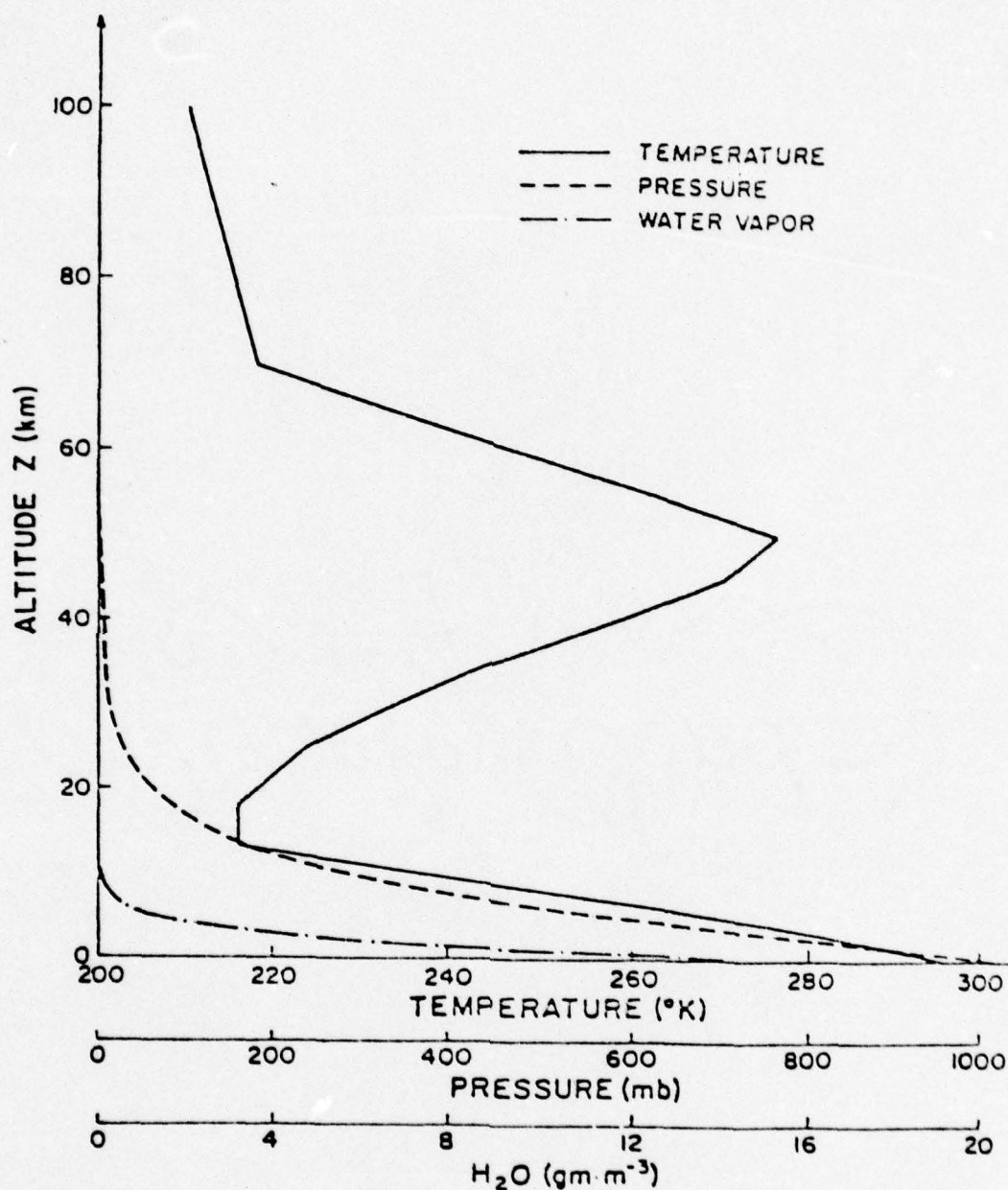
Figure 3. The mid-latitude summer atmospheric profile employed in calculating the reflected and transmitted radiances emergent from the cloud layers in data sparse areas.
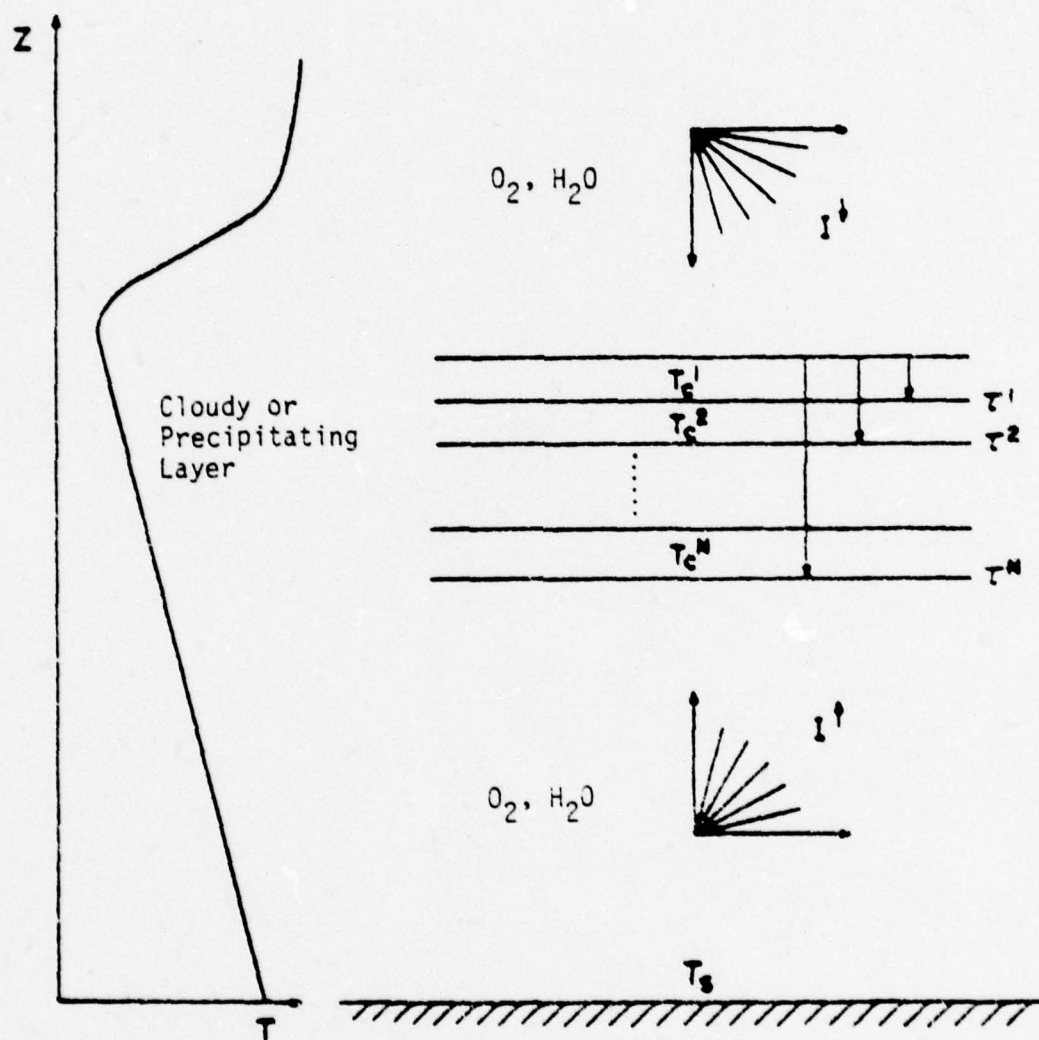
Figure 4. A model of the non-isothermal cloud or precipitating layer. The temperature within each predivided layer is assumed to be isothermal.

$$N(D) = N_o \, e^{-\Lambda D}, \tag{2}$$

where N(D)dD is the number of drops per unit volume with diameter between D and D+dD. Λ is the slope of the distribution curve, dependent upon the rainfall rate, and is given by

$$\Lambda(R) = 41 \, R^{0.21}, \tag{3}$$

where the rainfall rate R is measured in mm per hour and Λ is in units of cm^{-1}. The intercept parameter N_o is a constant with a value of 0.08 cm^{-4}. This exponential behavior of drop size distribution has been experimentally verified by Gunn and Marshall (1958) and Sekhon and Srivastava (1970).

To calculate the upwelling radiances at the top of the atmosphere the absorption and emission characteristics of the atmosphere must be parameterized. In the portions of the microwave spectrum under study here, oxygen and water vapor are the principal gases affecting the transmittance of radiation. These two gases combine to determine the transmittance at any given level of the atmosphere.

The absorption coefficient γ for oxygen is a function of frequency ν, pressure P, and temperature T as follows (Meeks and Lilley, 1963)

$$\gamma(\nu, P, T) = C_1 P T^{-3} \nu^2 \sum_N S_N \exp(-E_N/kT) \tag{4}$$

where C_1 is a constant representing the normal concentration of O_2, N the number of layers in the atmosphere, S_N a series of constants based on the frequency and layer number, and the exponent in the Boltzman

factor may be expressed by

$$E_N/kT = 2.06844 \, N(N+1)/T. \tag{5}$$

Equation (4) can be solved for each layer of the atmosphere.

The water vapor effect has been studied by Liebe (1969) and may be expressed as the attenuation per unit distance α,

$$\alpha = (4\pi\nu/c) \, n(\nu) \times 10 \, \log_{10} e, \tag{6}$$

where c is the speed of light and $n(\nu)$ the frequency dependent extinction coefficient. VanVleck (1974) calculated that a residual attenuation effect should be added to Eq. (6),

$$\alpha_R \approx 1.9 \times 10^{-9} \, p_w \, \nu^2/T^{5/2} \tag{7}$$

where p_w may be converted to water vapor density by

$$\rho_w = (288.75/T) \, p_w. \tag{8}$$

The water vapor and oxygen absorption coefficients are added together to obtain the absorption coefficient $\gamma_\nu(P)$ for each layer. These coefficients are then used to determine the transmittances at each layer using the relationship

$$T_\nu(P) = \exp\{-\sum_{i=N-1}^{o} \frac{1}{2}[\gamma_\nu(P_i) + \gamma_\nu(P_{i+1})]\Delta P\}, \tag{9}$$

where $P_N=0$ and $P_o=$surface pressure. The transfer program includes corrections to the transmittances for antenna gain effects and for the angular dependence of the absorption coefficients (Wolfe, private communication). From the transmittances, the weighting function may

be obtained, as shown in Figure 1 for the three oxygen channels.

The single scattering parameters were also calculated for the five SCAMS channels which were used in the transfer calculations. The Mie scattering program for polydisperse spheres developed by Liou and Hansen (1971) was employed to perform the single scattering calculations. The input parameters, and resulting scattering parameters are listed in Table 2.

Table 2. Input and Results of the Mie Scattering Program

Parameter		Channel				
		1	2	3	4	5
Input	ν (cm^{-1})	.7413	1.0470	1.7636	1.7953	1.8484
	n_r	5.07	4.36	3.21	3.16	3.07
	n_i	2.79	2.56	1.90	1.87	1.82
Cumulus Cloud	β_{ext}(km^{-1})	.001	.002	.003	.003	.003
	$\tilde{\omega}_\nu$	.3579	.3916	.7436	.7522	.7658
Precipitation (2mm per hour)	β_{ext}(km^{-1})	.005	.008	.018	.018	.018
	$\tilde{\omega}_\nu$	.2218	.2796	.3911	.3974	.4016
Precipitation (4mm per hour)	β_{ext}(km^{-1})	.008	.016	.030	.030	.030
	$\tilde{\omega}_\nu$	.1048	.1261	.2073	.2108	.2173

In Table 2, n_r and n_i are the real and imaginary indices of refraction, respectively. These values were derived by Gunn and East (1954) and interpolated and extrapolated to the correct frequencies. β_{ext} is the extinction coefficient obtained by multiplying the true cross section per particle for extinction by the number of particles per unit area and unit height. The local albedo of single scattering

$\tilde{\omega}_\nu$ may be expressed as

$$\tilde{\omega}_\nu = \frac{\beta_{sca}}{\beta_{ext}} ,$$ (10)

where β_{sca} is the volume cross section for scattering for a polydispersion (Deirmendjian, 1969).

It is important to note the increase in β_{ext} with frequency over the SCAMS frequency range, and its increase with the increase in cloud particle size and density. The single scattering albedo $\tilde{\omega}_\nu$ also increases with frequency, but decreases with the larger particle size.

CHAPTER 3

MICROWAVE RADIATIVE TRANSFER IN A SCATTERING ATMOSPHERE

3.1 Basic Equations

The basic transfer equation for a plane parallel cloud layer in
local thermodynamic equilibrium for a monochromatic microwave radia-
tion field may be written in the form

$$\mu \frac{dI_\nu(\tau,\mu)}{d\tau} = I_\nu(\tau,\mu) - \frac{\tilde{\omega}_\nu}{2} \int_{-1}^{+1} P_\nu(\mu,\mu') I_\nu(\tau,\mu') d\mu' - (1-\tilde{\omega}_\nu) B_\nu[T(\tau)],$$

(11)

where I_ν represents the monochromatic radiance of frequency ν, μ the
cosine of the emergent angle with respect to the zenith, τ the optical
depth, T the cloud temperature which is a function of cloud height or
optical depth, P_ν the normalized axially symmetrical phase function, $\tilde{\omega}_\nu$
the single scattering albedo. Included in the emission term in Eq.
(11) is the Planck function, expressed in the frequency domain by

$$B_\nu(T) = \frac{2h\nu^3}{c^2(e^{h\nu/KT}-1)}$$

(12)

where h and K are the Planck's and Boltzman's constants, respectively,
and c is the speed of light.

The normalized phase function can be expanded in Legendre poly-
nomials of finite terms. Upon replacing the integration in Eq. (11)
by summation utilizing the Gauss' quadrature formula, a set of first

order inhomogeneous differential equations can be derived. By seeking the homogeneous and particular solutions of the differential equations as outlined by Chandrasekhar (1950), the complete solutions of the scattered intensity for an isothermal cloud temperature T_c at a given discrete-stream i may be expressed in the form

$$I_\nu(\tau,\mu_i) = \sum_m L_m \phi_m(\mu_i) e^{-k_m \tau} + B_\nu(T_c) \tag{13}$$

where $\sum_m$ represents summation over the discrete streams employed, ϕ_m and k_m are eigenfunction and eigenvalue of the differential equations and L_m are a set of constants of proportionality to be determined from the radiation boundary conditions.

In the microwave domain, the Rayleigh-Jeans approximation of the Planck function for emitted radiation is customarily used and is given by

$$B_\nu(T) \approx 2KT\nu^2 c. \tag{14}$$

In addition, since the radiometers used to measure thermal emission are usually calibrated using sources at set reference temperatures, the output is normally expressed in terms of an equivalent temperature, the brightness temperature $T_B(\nu)$, defined as

$$I_\nu \approx 2\nu^2 cKT_B(\nu). \tag{15}$$

Using this relationship, the fundamental transfer equation, Eq. (11), may be rewritten in terms of the brightness temperature

$$\mu \frac{dT_B(\nu)}{d\tau} = T_B(\nu) - \frac{\tilde{\omega}_\nu}{2} \int_{-1}^{+1} P(\mu,\mu') T_B(\nu) d\mu' - (1-\tilde{\omega}_\nu) T(\nu), \tag{16}$$

where $T_B(\nu)$ is a function of μ and τ, and $T(\nu)$ a function of τ only. Also, the solution of the transfer equation may now be expressed in terms of brightness temperature, thus

$$T_B(\nu) = \sum_m L_m \phi_m(\mu_i) e^{-k_m \tau} + T_c(\nu), \qquad (17)$$

where the constants of proportionality L_m are different from those of Eq. (13) and may be obtained through the use of the radiation boundary conditions. T_c is the cloud layer temperature.

At the cloud top, the downward intensity is equal to the radiation emitted by the gaseous, non-scattering atmosphere above the layer, so that

$$T_B^1(\nu) = \int_z^\infty T(z) d\tau_\nu (z, z_t; -\mu_i), \qquad (18)$$

where z_t denotes the cloud top height. Within the cloud layer, where scattering does occur, continuity of the radiances from all directions is required, thus,

$$T_B^\ell(\nu) = T_B^{\ell+1}(\nu), \qquad \ell = 1, 2, \ldots, N-1, \qquad (19)$$

where N is the total number of sublayers within the cloud. At the lower boundary of the cloud layer, the upwelling radiance is generated by three sources:

    a) the radiation emitted from the surface, determined by the surface emissivity ε_s and the surface temperature T_s,

    b) reflection from the surface of the downwelling radiance from

the cloud layer, and

c) the upward gaseous, non-scattering atmospheric contribution to the bottom of the cloud layer, that is

$$T_B^N(\nu) = \varepsilon_s(\nu)T_s(\nu)\tau_\nu(z_b,0;\mu_i)$$

$$+ [1-\varepsilon_s(\nu)]\tau_\nu(z_b,0;\mu_i) \int_{z_b}^{0} T(z)d\tau_\nu(z,z_b;-\mu_i)$$

$$+ \int_{0}^{z_b} T(z)d\tau_\nu(z_b,z;\mu_i), \tag{20}$$

where z_b represents the cloud base height, $T(z)$ is the atmospheric temperature as a function of height, and the transmittance is defined as

$$\tau_\nu(z_2,z_1;\mu_i) = \exp[- \frac{1}{\mu_i} \int_{z_1}^{z_2} K_\nu(z)n(z)dz], \tag{21}$$

where $K_\nu(z)$ and $n(z)$ represent the absorption coefficient and number density, respectively, of the absorbing gases at height z. It should be noted that for precipitating clouds, the scattering layer will extend to the surface, and there will be no contribution from atmospheric emission. Thus, Eq. (20) reduces to

$$T_B^N(\nu) = \varepsilon_s(\nu)T_s(\nu). \tag{22}$$

The solution of the microwave radiative transfer equation given by Eq. (17) is applicable only to isothermal and homogeneous cloud layers. To apply the transfer solution to the multilayered cloud system, we divide the cloud layers into a number of sub-layers, each of

which is considered to be isothermal and homogeneous. By matching the radiation continuity equation for radiances in each sub-layer, a set of linear equations with unknown coefficients may be determined by standard matrix inversion methods. A similar procedure has been employed by Liou (1975) to evaluate the transfer of solar radiation in inhomogeneous atmospheres. This technique has also been used by Feddes and Liou (1977, 1978) to investigate the transfer of spectral infrared radiation in cloudy atmospheres.

The microwave transfer program in cloudy atmospheres described above will yield the upward radiance in terms of the brightness temperature at the cloud top, $T_B(\nu, z_t)$. From this information, the brightness temperature from a satellite point of view in a completely cloudy condition becomes

$$T_B^C(\nu, \infty) = T_B(\nu, z_t) \tau(\infty, z_t; \mu_i) + \int_{z_t}^{\infty} T(z) d\tau_\nu(\infty, z; \mu_i). \tag{23}$$

Also, for cloud-free, non-scattering atmospheres in local thermodynamic equilibrium, the calculated brightness temperature at the top of the atmosphere is simply given by

$$T_B^{NC}(\nu, \infty) = \epsilon_s(\nu) T_s(\nu) \tau_\nu(\infty, 0; \mu_i)$$

$$+ [1 - \epsilon_s(\nu)] \tau_\nu(\infty, 0; \mu_i) \int_{\infty}^{0} T(z) d\tau_\nu(z, \infty; -\mu_i)$$

$$+ \int_{0}^{\infty} T(z) d\tau_\nu(\infty, z; \mu_i). \tag{24}$$

3.2 Problem of Surface Emissivity

A special problem area in the use of microwaves for atmospheric sensing is surface emissivity. In the infrared spectrum, emissivity values of the earth's surface in the microwave spectrum vary over a considerable range, from 0.4 to 1.0 (Gloersen, et al., 1972). The emissivity of the sea surface typically ranges between 0.4 and 0.5, dependent upon such variables as salinity, sea ice, surface roughness, and sea foam. In addition, there is a frequency dependence, with higher frequencies displaying higher emissivity values. Of more importance in this research, however, are the variations of emissivity over land surfaces.

Since the SCAMS antenna beamwidths give ground resolutions of between 145 km at nadir and 330 km at maximum scan angle, the surface emissivity sensed from the satellite is of necessity a mean value, averaged over the individual scan. This is convenient for our purposes, as small discontinuities such as small bodies of water, do not seriously affect the overall reading, while large scale changes, such as surface wetting from precipitation, do cause a detectable change. With this size of scan, other variables, such as density, surface roughness, vegetation and orography tend to be smoothed, leaving only the effects of moisture to cause emissivity changes.

In an extensive investigation, Schmugge, et al. (1974) performed calculations to determine the effect of soil moisture on emissivity values. He also verified the Fresnel method of calculating emmisivities. By assuming an electromagnetically smooth surface, Kirchoff's Law may be applied such that the emissivity is equal to the surface absorptivity or

$$\varepsilon_s(\nu) = 1 - r_s(\nu). \tag{25}$$

From Fresnel's law, the surface reflectivity may be calculated for the vertically and horizontally polarized components, $r_1(\nu)$ and $r_2(\nu)$ (see e.g. Born and Wolfe, 1969),

$$r_1(\nu) = \frac{\cos i - n \cos t}{\cos i + n \cos t}$$
$$r_2(\nu) = \frac{n \cos i - \cos t}{n \cos i + \cos t} \tag{26}$$

where i and t are the incident and reflected angles and n is the index of refraction. Equation (26) may be reduced by the use of Snell's law,

$$\sin t = \sin i/n \tag{27}$$

The index of refraction n is directly related to the dielectric properties of the surface. Since the dielectric constant of dry soil is much smaller than that of water in the microwave region, the dielectric properties of any given soil depends heavily on the moisture content of that soil. Edgerton et al. (1971), determined that wetting of a soil surface would result in a rapid decrease in emissivity, on the order of 2% to 5%. Using this information, and independent verification, Gloersen, Wilheit and Schmugge (1972) found that emissivity values for dry soil may be assumed to be .95 - .97 and for wet soil .92 - .95.

In the theoretical studies conducted with the computer model during this research, a number of different emissivity values were used and then compared with the observed results. These tests confirmed

the Gloersen figures for both wet and dry soils, and these emissivity values were used for all subsequent calculations.

CHAPTER 4

COMPARISONS BETWEEN CALCULATED AND OBSERVED BRIGHTNESS
TEMPERATURES FOR SELECTED ATMOSPHERIC CONDITIONS
AND SENSITIVITY ANALYSES

4.1 Data Selection

The basic criteria for selection of the data used as input to the
SCAMS program was for the surface and radiosonde data to be readily
available and to match the time and location of the satellite overpass.
Additionally, the scans must be in the presence of synoptic scale wea-
ther so as to provide a variety of cloud and weather conditions.
Points at or near nadir were chosen to ensure the least error in
applying the real data to the theoretical calculations, since the theo-
retical upwelling radiances would be most accurate at nadir.

Using these criteria, 64 data points were selected at or near the
satellite subtrack on five consecutive days from August 21 through 25,
1975. The points were selected if a radiosonde sounding was available
within 100 km of the center of the scan, the surface weather analysis
for the scan was available, and the time of the pass was within six
hours of the time of both of the previous requirements. Since Nimbus
6 has an equator crossing time of approximately 1800Z (GMT) for the
United States passes, the 1200Z surface analyses and radiosonde sound-
ing data were used. During the five-day period, 21 clear cases, 23
cloudy nonprecipitating cases, and 20 cloudy precipitating cases were

plotted.

The synoptic situation during this time period was a typical mid-summer pattern. High pressure and clear skies dominated the southern United States while a series of low pressure systems moved eastward across the northern half of the country, causing large areas of showers and rain. No severe weather occurred during the period. Most of the clear cases were from the southern area, but seven were selected in the northern states. The cloudy cases were predominantly from the northern states, and included three southern Canadian stations. The precipitating cases followed the same pattern as the cloudy cases.

The accuracy of the surface measurements is the same as for all surface data collected by the National Weather Service. The radiosonde water vapor data are estimated to be accurate within 10 percent, and the temperature readings are accurate to within $0.5^{\circ}C$.

4.2 Clear Atmosphere Conditions

Prior to the calculation of the sensitivity analysis data, a test was made to determine the accuracy of the clear column radiance (CCR) program. To test the ability of the program to generate CCR values similar to those observed by the Nimbus 6 SCAMS channels, a number of test cases were selected. Each case was chosen such that the surface weather records for the station indicated a clear atmosphere at the time of the satellite pass. The radiosonde data (temperature, pressure, and mixing ratio) were read into the CCR program and used to generate expected CCR values for the five SCAMS channels. These expected values are plotted against the observed values in Figure 5.

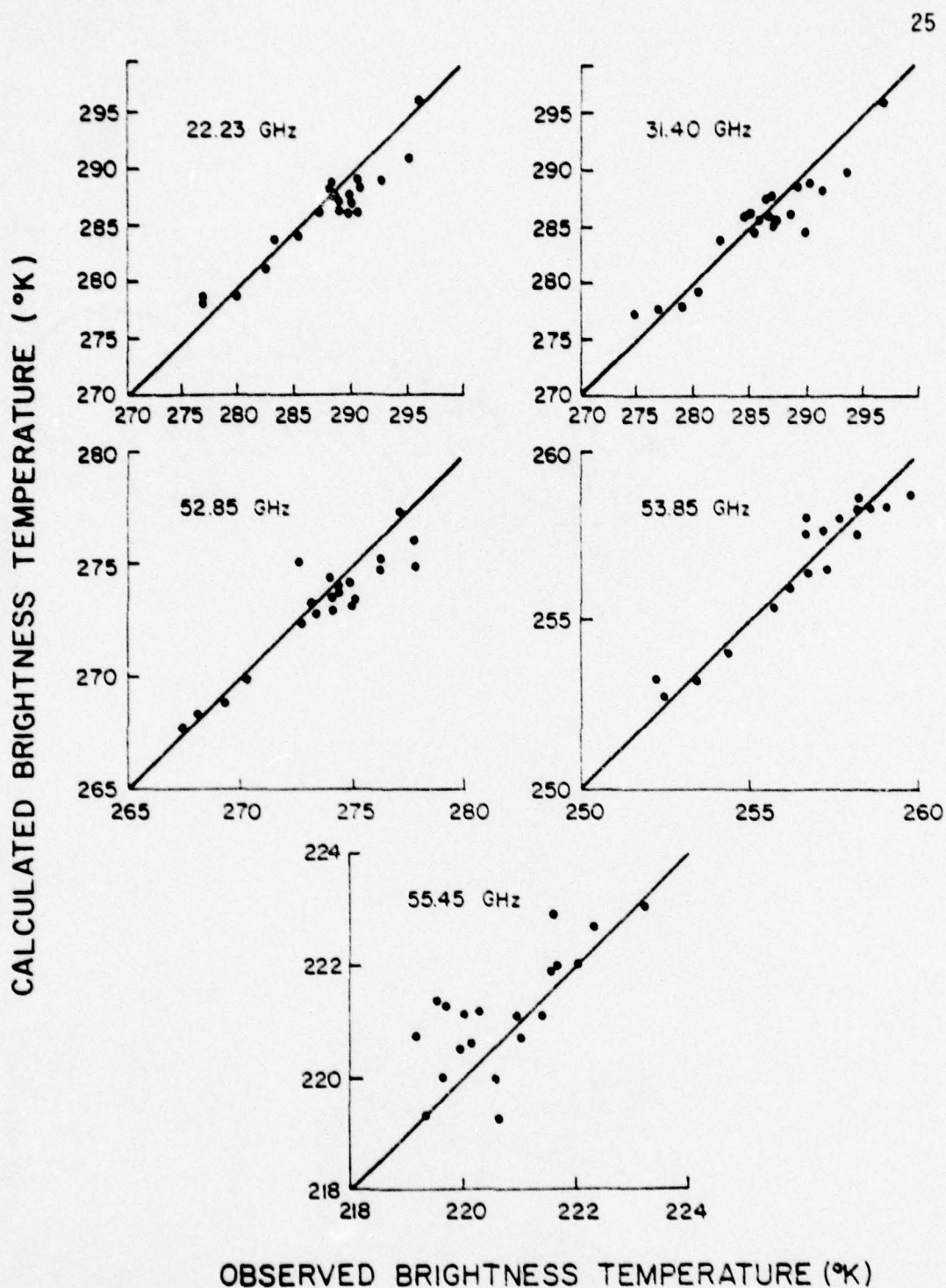For channels one through five, emissivity values of .95, .96, .97,

Figure 5. Calculated and observed brightness temperatures for clear atmospheric conditions. Scales of brightness temperatures are varied to best reflect each channel.

.97, .97 were used, respectively. As explained in Chapter 3, these values provide the best estimate of dry soil emissivities, particularly over vegetated areas. A study of the sensitivity of brightness temperatures to emissivity values is included later in this chapter.

The standard deviations of the calculated values for the five channels are 1.06°, 1.29°, $.73^{\circ}$, $.42^{\circ}$ and $.29^{\circ}$ respectively. Since instrument error for each of the five channels would be expected to be 2.87°, 2.86°, 2.74°, 2.57° and 2.21° respectively, the CCR calculated values may be assumed to be accurate.

Having established the accuracy of the program in a clear atmosphere, the next step is to conduct a similar analysis for each channel in a variety of cloudy and precipitating atmospheres.

4.3 Cloudy and Precipitating Conditions

To test the ability of the transfer program to generate correct upwelling radiance values, as observed by the Nimbus 6 SCAMS radiometer, a number of test cases were again selected. Each case again had to have a timely radiosonde sounding and surface weather report, coinciding with the satellite pass. These cases were used to verify that the theoretical calculations for cloudy and precipitating conditions do represent the satellite observations accurately.

The cloudy cases were selected such that each case was overcast by low or middle clouds, with no precipitation currently or in the previous six hours. The cases were further divided into thick and thin overcast, using the current weather observations as a guide. Each case was then processed through the transfer program, using a one kilometer nonprecipitating cloud for the thin overcast cases and

a four kilometer cloud for the thick overcast cases. The results are plotted against the satellite observed values for each case in Figure 6.

The Deirmendjian modified gamma distribution was used for the drop size distribution of the nonprecipitating cloud. As discussed in Chapter 2, the upwelling radiance was found not to be sensitive to the type of distribution used. Additionally, sensitivity analyses are included later in this chapter which demonstrate that the height of the base of the low cloud does not have a significant effect on the upwelling radiance. The same dry soil emissivities listed for the clear case were used.

The standard deviations of the calculated values from the observed upwelling radiance for channels 1 through 5 are 1.83^o, 1.80^o, $.82^o$, $.73^o$ and $.34^o$ respectively. These deviations are larger than in the clear atmosphere verifications but still well within the expected instrument error of the radiometer. The most apparent reason for the increased variance would be the inherent error of assigning an arbitrary scale of cloud thickness to a variety of real cases with current weather observations.

The precipitating cases were selected in the same manner as the cloudy cases, with the exception that the observation must have shown precipitation at the time of the satellite pass, and the rainfall rate must have been obtainable from the surface weather observations. These cases were divided into four sub-groups, depending on the observed rainfall rate. Each case was then processed through the transfer program, using the proper parameters for the individual rainfall rate, and the actual radiosonde sounding data for the atmospheric
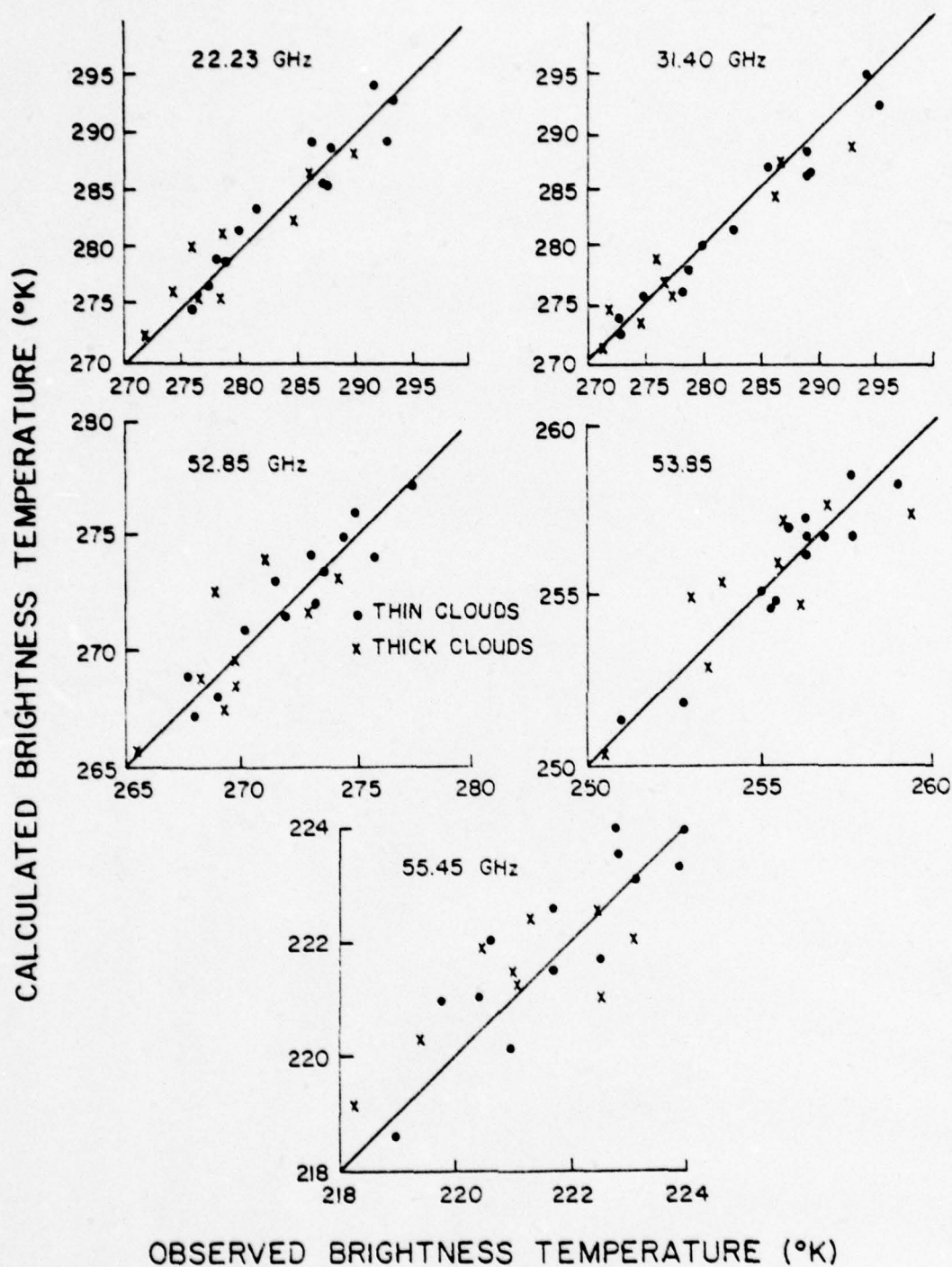
Figure 6. Calculated and observed brightness temperatures for cloudy atmospheric conditions. Scales of brightness temperatures are varied to best reflect each channel.

profile. The results are plotted against the satellite observed up-welling radiances for each case in Figure 7.

For precipitating conditions, lower surface emissivity values were used, as explained in Chapter 3. Values of .93, .94, .95, .95, and .95 for channels one through five, respectively, were chosen. Sensitivity analyses to the variable are conducted later in this chapter.

The standard deviations of the calculated values from the observed upwelling radiances for channels one through five are 1.56^O, 1.42^O, $.80^O$, $.66^O$ and $.34^O$, respectively. These deviations fall between the clear and cloudy case verification deviations. This is most probably due to the inaccuracy resulting from assigning a single rain-rate for a one mm per hour range of precipitation rates. It is important to note that the results still fall within the expected instrument error, thus verifying the accuracy of the transfer program in duplicating upwelling radiances for precipitating condition. The next step is to determine the sensitivity of the channels to the various input parameters.

4.4 Theoretical Sensitivity Analysis

To conduct sensitivity analysis of the upwelling radiance at the top of the atmosphere in cloudy and precipitating conditions, a series of different conditions were inserted into the transfer program. The resulting upwelling radiances at the top of the atmosphere were then plotted as a function of the variable under study. These variables include surface emissivity, cloud base height, cloud thickness of nonprecipitating clouds, and rainfall rate. The results of these
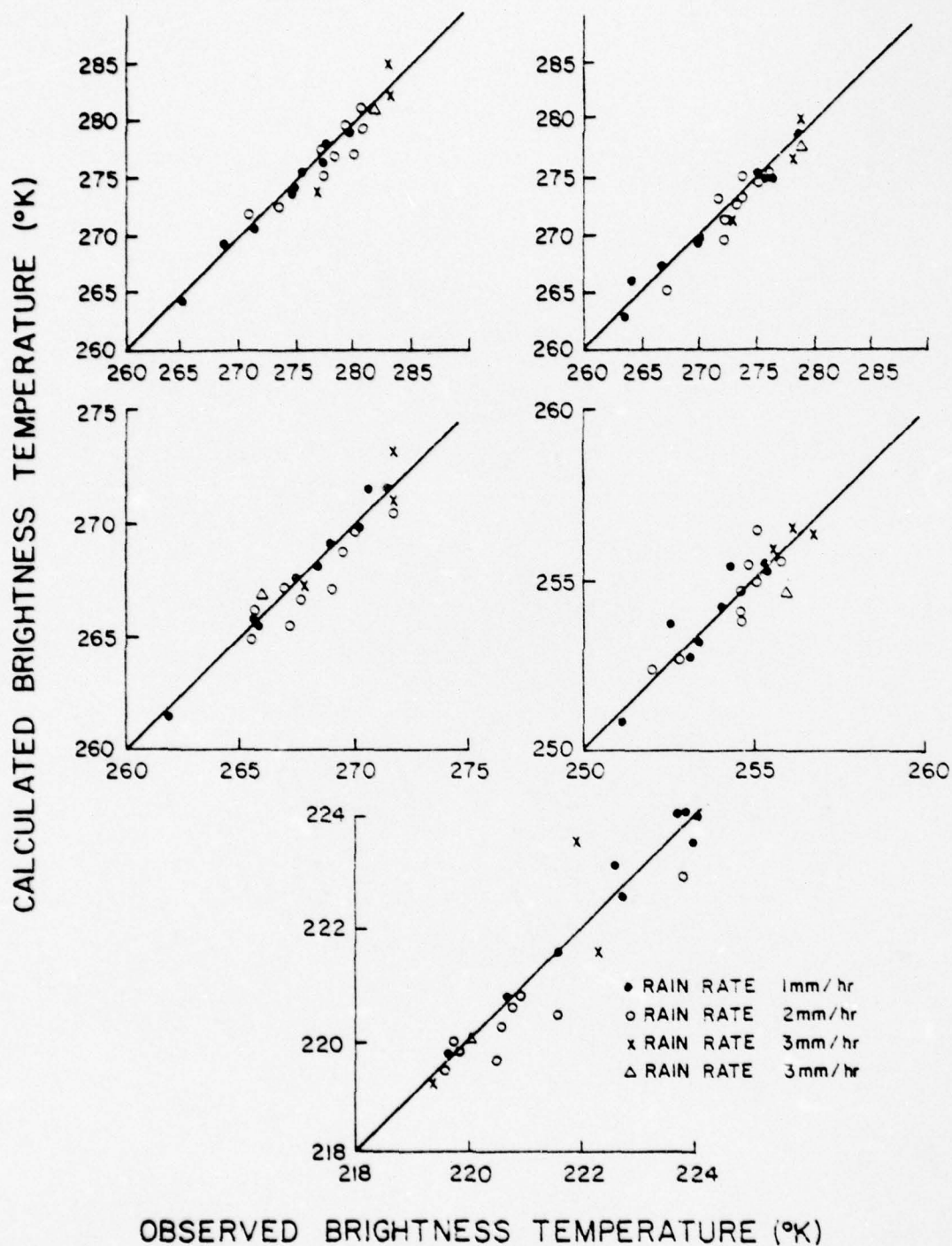
Figure 7. Calculated and observed brightness temperatures for precipitating atmospheric conditions. Scales of brightness temperatures are varied to best reflect each channel.

calculations are displayed in Figures 8, 9, 10 and 11. In each case, a standard summer mid-latitude atmospheric profile similar to that shown in Figure 3 was used, with all parameters held constant except the specific variable under consideration.

The first sensitivity analysis shown is the effect of surface emissivity on the upwelling radiance in both clear and precipitating atmospheres, displayed in Figure 8. The emissivity was varied from .75 to 1.00, to cover all normally expected values for soil and vegetated surfaces. The difference in slopes between the two cases would appear to be due to the increased absorption by the precipitating cloud at higher radiance levels. It is interesting to note the differences in the slopes of the emissivity lines between the channels. Channels one and two, which most clearly sense the surface, are most affected by changes in emissivity, channel three is less affected, while channels four and five, where the atmosphere is almost opaque, are affected very little.

Next the effects of varying the base height of a given nonprecipitating cloud on the expected upwelling radiance at the top of the atmosphere was studied. In all five channels, varying the cloud base height from one kilometer up to five kilometers has less than a 1.0% effect upon the upwelling radiance. Thus, the height of low and middle clouds would appear to have a negligible effect, in fact the effect should be predominantly hidden in the random instrument error of the radiometer.

Figure 9 displays the relationship between the expected upwelling radiance and the thickness effect of a low (base height of two kilometers) nonprecipitating cloud. These calculations were obtained for
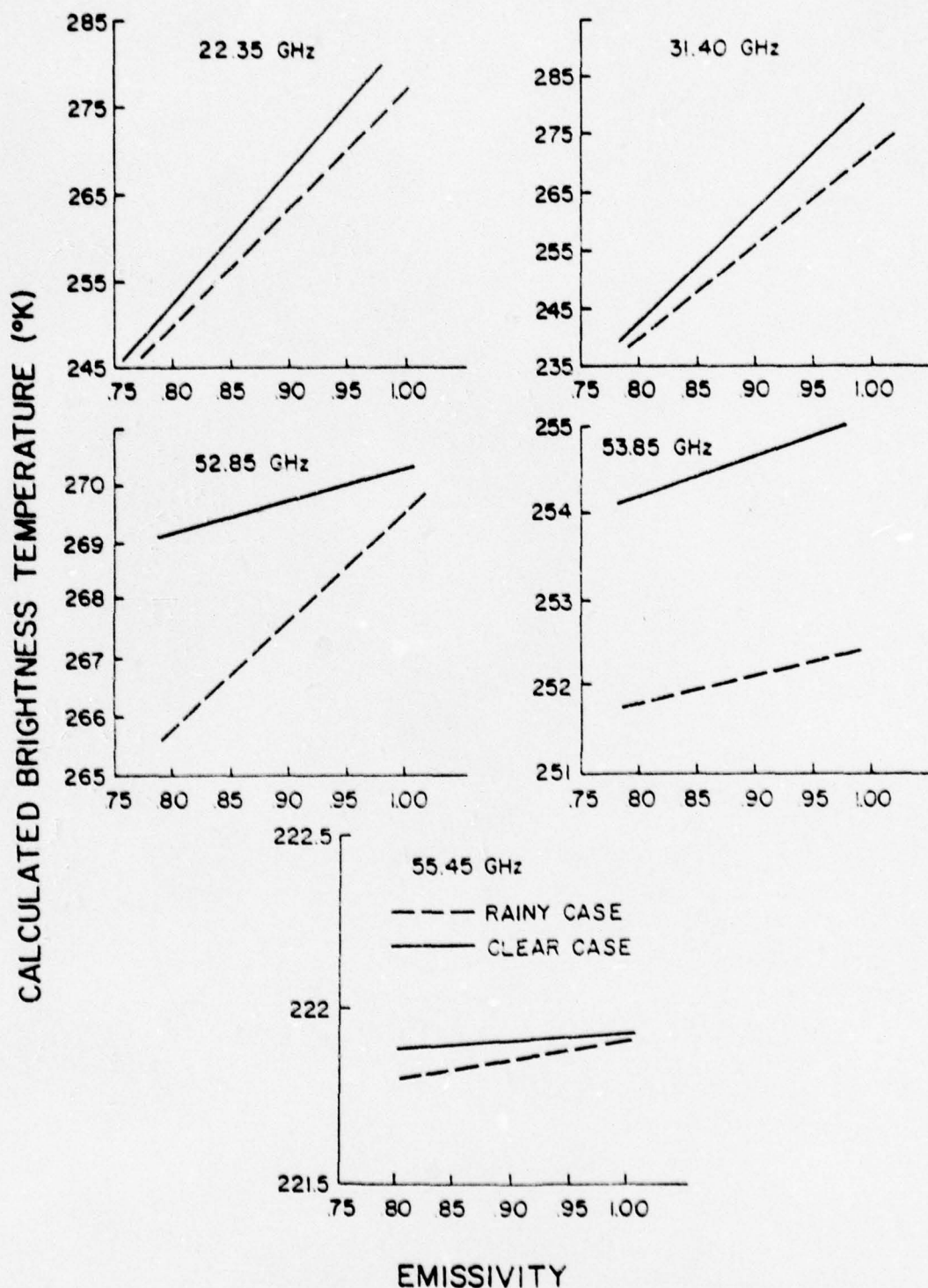
Figure 8. Calculated brightness temperatures at varying surface emissivities for clear and precipitating atmospheric conditions. Scales of brightness temperatures are varied to best reflect each channel.

33
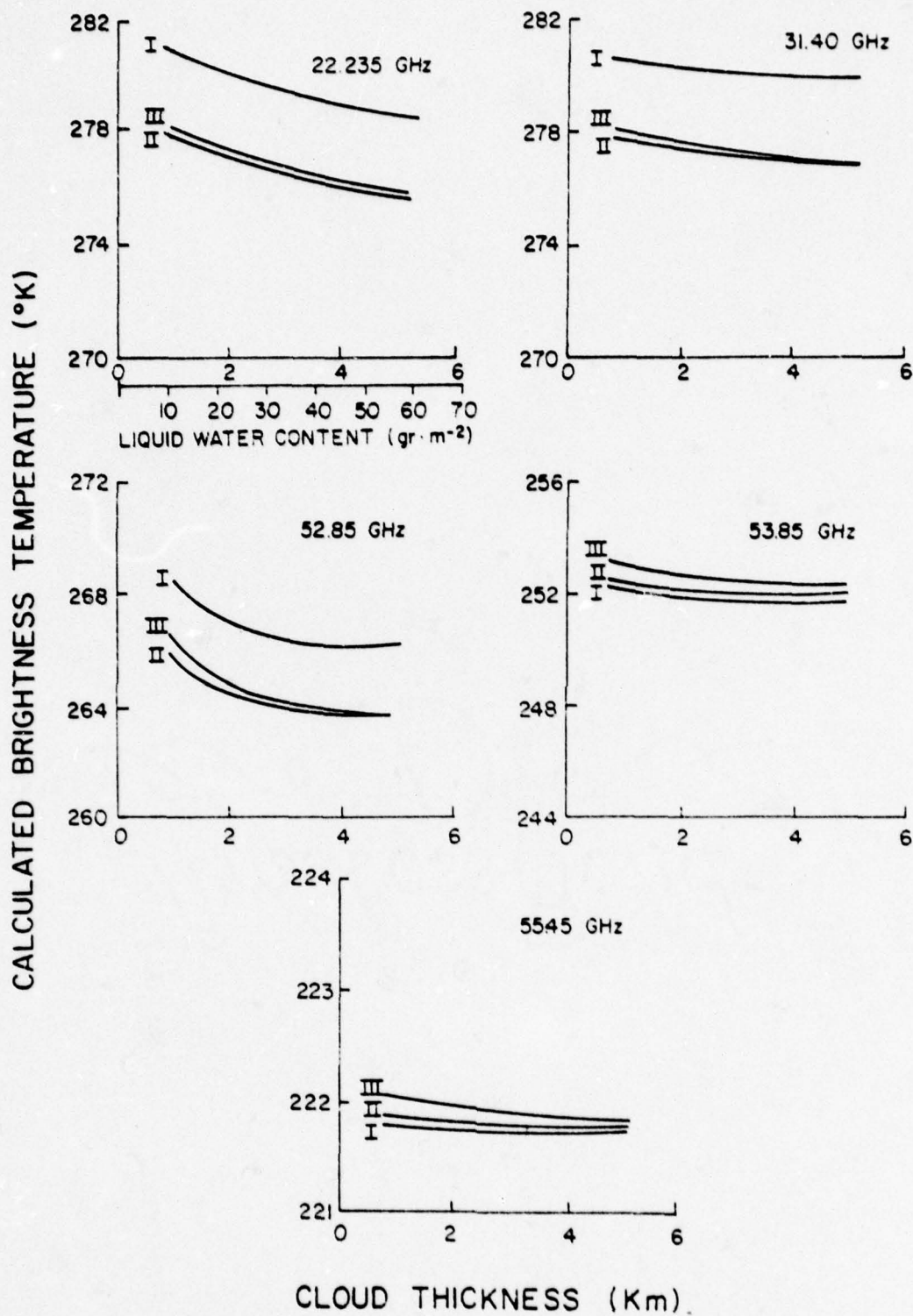
Figure 9. Calculated brightness temperatures resulting from increasing the thickness of a low nonprecipitating cloud for three different atmospheric profiles.
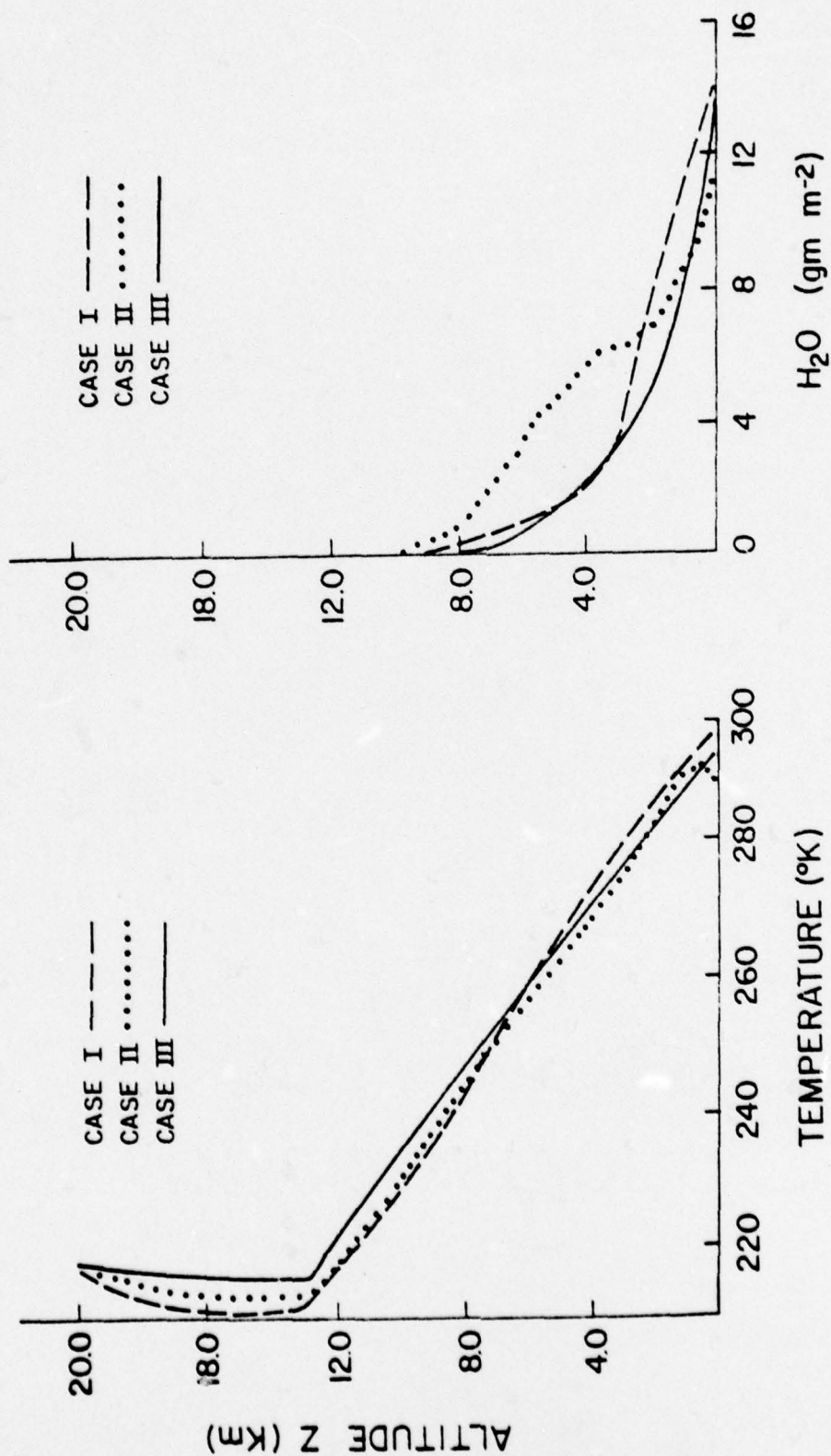
Figure 10. The three low-level (below 20 km) atmospheric profiles employed in Figures 9 and 11.
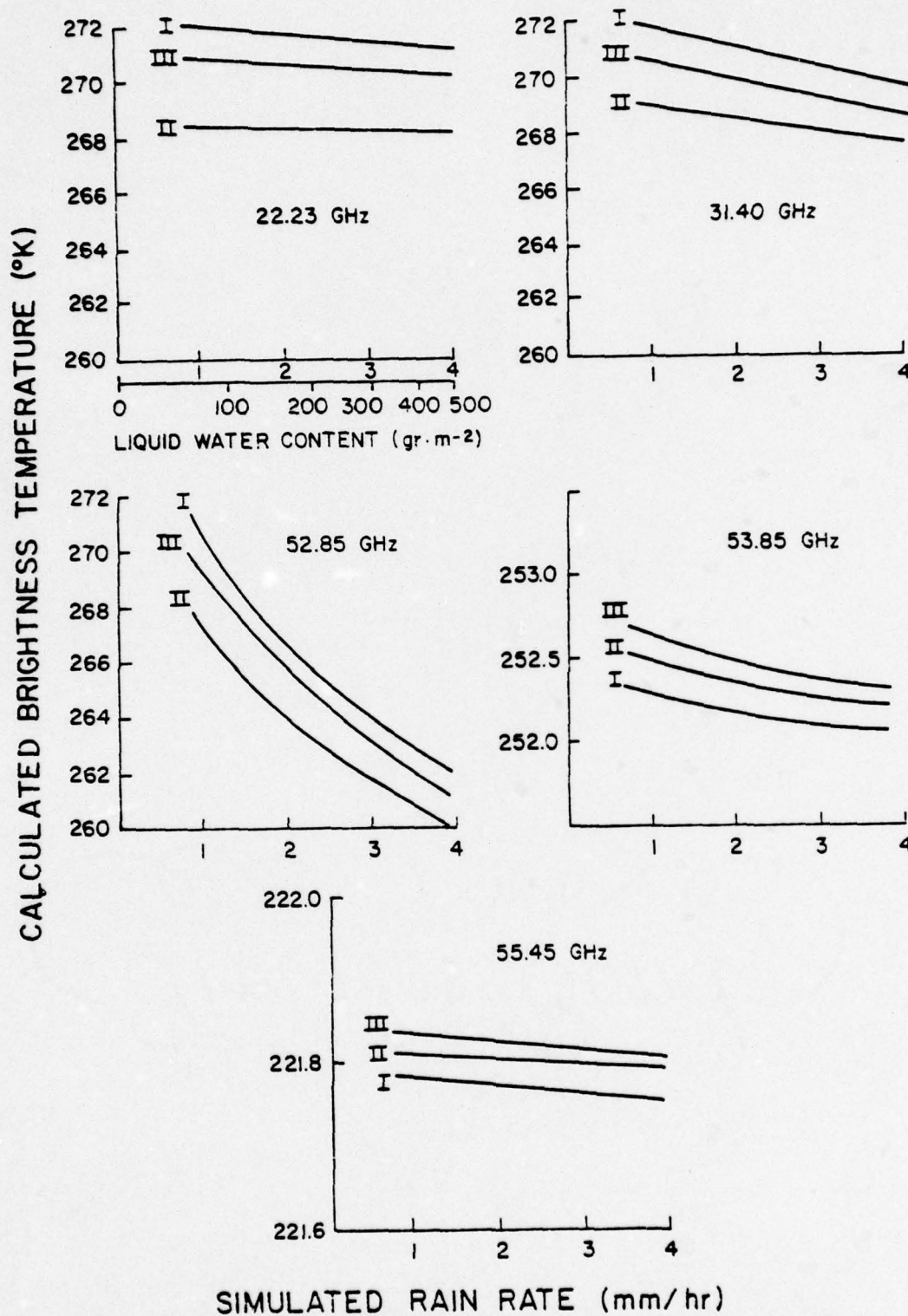
Figure 11. Calculated brightness temperatures resulting from varying the rainfall rate (or liquid water content) for three different atmospheric profiles.

three atmospheric profiles, which are graphically displayed in Figure 10. For the cloud type, a modified gamma drop size distribution developed by Deirmendjian (1969) described in Chapter 2 was selected. As described earlier, no significant effect was noted resulting from using a different size distribution. In the channels centered at 53.85 GHz and 55.45 GHz, the effect of nonprecipitating low clouds may clearly be neglected, but the other channels are to varying degrees affected by the cloud layer. Previous temperature profile retrieval methods (Waters et al., 1975; and Staelin et al., 1975) have made the most basic of assumptions concerning the effects of clouds within the field of view, e.g., that the clouds had no effect at all on the observed temperature data. Figure 9 shows that this assumption may not be correct. Errors on the order of 1.0%-2.0% can be introduced by this assumption. Clearly, an accurate temperature retrieval method using satellite microwave data should include a compensatory mechanism for temperature soundings in cloudy atmospheres.

Figure 11 plots the expected upwelling radiance for three precipitating cloudy atmospheres with different rainfall rates. The temperature and moisture profiles are as shown in Figure 10. This figure assumes that the surface is wet, and thus has a lower emissivity than if it were dry, as was assumed for the previous figures. Drop size distribution is an important parameter used to obtain the proper scattering properties of the hydrometers. We chose the theoretical drop size distribution developed by Marshall and Palmer (1948) described previously.

By assigning a series of values for rainfall rate R to the raindrop size distribution, calculating the scattering parameters shown in

Table 2, and testing each case on a standard atmospheric profile, Figure 11 was developed. The only channel which shows a significant effect as the rainfall rate is increased is the channel centered at 52.85 GHz. This channel shows a dramatic drop, on the order of $10^{O}K$, for a rainfall rate increase from one mm per hour to four mm per hour.

Figure 12 is a plot of the calculated brightness temperature expected from varying water vapor concentrations for channels one and two. Variations in water vapor have no significant effect upon channels three, four or five. Increase in water vapor concentration has the strongest effect on channel one, centered on 22.235 GHz, a weak water resonance. This channel, when compared to the spectral window channel two at 31.40 GHz, has been used to infer water vapor abundance over ocean surfaces (Staelin et al., 1976; Wilheit et al., 1977). Figure 12 suggests that a similar relationship may be discerned over land masses.
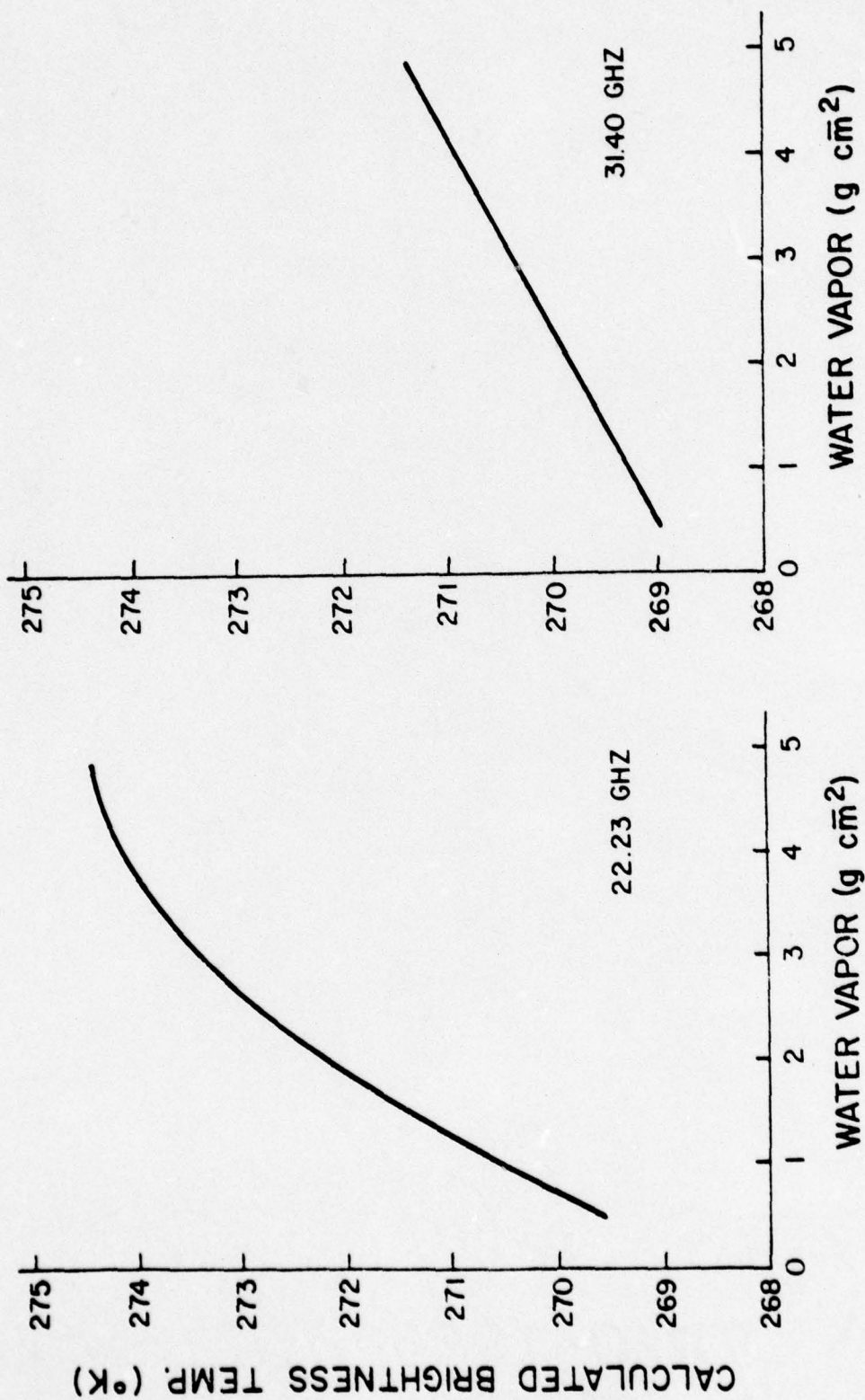
Figure 12. Calculated brightness temperatures for SCAMS channels 1 and 2 resulting from varying the amount of water vapor in an atmospheric profile.

CHAPTER 5

LIQUID WATER CONTENT AND RAINFALL RATE DETERMINATION
FROM SCAMS CHANNELS

This chapter will contain the development of empirical formulas
for the estimation of atmospheric liquid water and water vapor con-
tent from SCAMS data. Included will be a synoptic discussion and maps
and satellite photographs for the days used for the discussions.
Finally, there will be a comparison of the results obtained from the
formulas with both observed data and previous infrared studies.

5.1 Empirical Formulas for the Derivation of
Liquid Water and Water Vapor Content

From inspection of the microwave spectrum, we find that below
40 GHz, the transmittance $\tau_\nu(\infty,0;\mu_i)$ is approximately unity (Grody,
1976) and thus the brightness temperature, as expressed in Eq. (24)
can be approximated by

$$T_B(\nu,\infty) \approx T_s[1-\tau_\nu^2(\infty,0;\mu_i)(1-\varepsilon_s(\nu))]. \tag{28}$$

In this range of frequencies, the atmospheric transmittance is due in
the main part to absorption by water vapor and liquid water, thus

$$\tau_\nu(\infty,0;\mu_i) = \tau_\nu(H_2O)\tau_\nu(Liquid). \tag{29}$$

To estimate the water vapor concentration W and the liquid water

content Q, we must have these transmittances expressed in a form using these quantities.

For frequencies below 50 GHz, the transmittance for water content consisting of water droplets with radius less than 50 μm may be expressed by the Rayleigh limit (Goldstein, 1951). Thus,

$$\tau(\text{Liquid}) \approx \exp(-Q/Q_0(\nu)) \approx 1 - Q/Q_0 \tag{30}$$

where $Q_0(\nu) = K\nu^2$, $K = 1.11 \times 10^{[0.0122(291-T_c)-4]}$ and T_c is the mean cloud temperature. This relationship is valid if $Q \ll Q_0$, that is, only below 50 GHz. For frequencies near 22 GHz we may also write

$$\tau(H_2O) \approx 1 - W/W_0(\nu), \tag{31}$$

because at these frequencies $W \ll W_0(\nu)$. These expressions may be substituted into Eq. (28) to obtain (neglecting higher order terms of Q and W),

$$T_B(\nu) \approx \varepsilon_s(\nu)T_s + 2(1-\varepsilon_s(\nu))T_s(Q/Q_0(\nu) + W/W_0(\nu)) \tag{32}$$

It is clear that, once a reliable estimate of surface temperature T_s and surface emissivity $\varepsilon_s(\nu)$ are obtained, W and Q may be obtained from the observed brightness temperature at two channels. The solution of Eq. (32) has the form

$$Q = q_0 + q_1 T_B(\nu_1) + q_2 T_B(\nu_2) \tag{33a}$$

$$W = w_0 + w_1 T_B(\nu_1) + w_2 T_B(\nu_2) \tag{33b}$$

where $T_B(\nu_1)$ and $T_B(\nu_2)$ are the brightness temperatures at frequencies

22.235 and 31.40 GHz, respectively, and the coefficients q_i and w_i are dependent upon the surface temperature and emissivity and may be determined through statistical linear regression.

For the SCAMS channels centered at 22.235 and 31.40 GHz, a three dimensional linear regression technique (Fryer, 1966) was used to determine the coefficients q_i and w_i in Eqs. (33a) and (33b). Atmospheric profiles obtained from the U. S. Weather Service Northern Hemisphere Data Tabulations were used to compute brightness temperatures using the procedures described in Chapter 3. Liquid water was added artificially to a selection of the atmospheres, in varying amounts in the same manner as for the sensitivity analyses presented in Section 4.4 to obtain the effects of liquid water on the brightness temperature. Emissivity values were treated as described in Chapter 3. An important difference between the Grody study and this research is the data base for the empirical formulas. While Grody based his equations on observed data, this research is based on the computer-generated data points, resulting in a more objective data sample.

The linear regression obtained forms of Eqs. (33a) and (33b) for water vapor and liquid water over the land surfaces are affected by the surface emissivity, which is in turn dependent on soil wetness. Examination of SCAMS data, computer analysis, and statistical verification results in an empirical decision matrix using observed brightness temperatures for SCAMS channels two and three, $(T_B(\nu_2)$ and $T_B(\nu_3))$, centered at 31.40 and 52.85 GHz, respectively, to determine surface characteristics. Table 3 displays the results of this analysis, which is shown graphically in Figure 13.
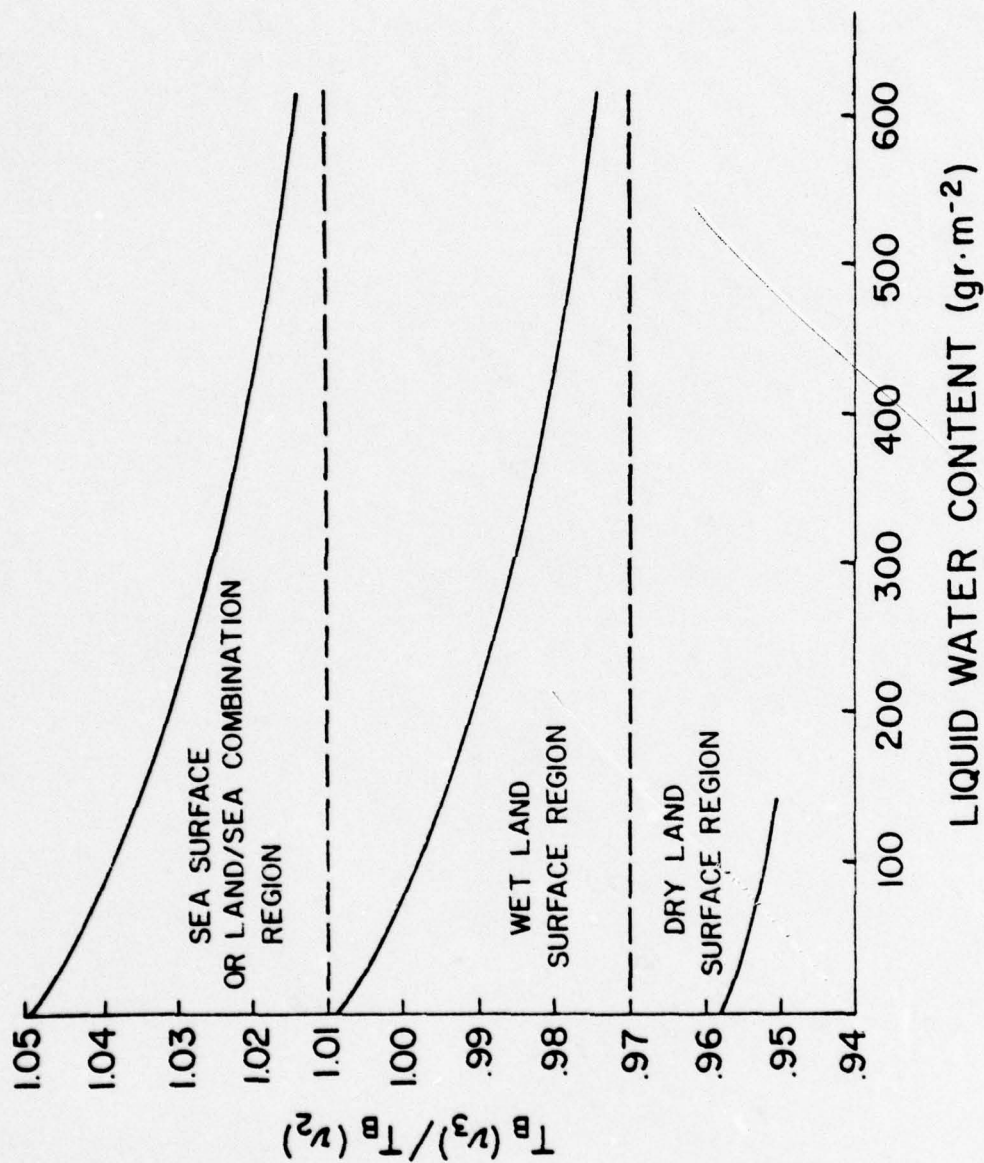
Figure 13. Calculated brightness temperature ratio between SCAMS channels 2 and 3 for different surfaces resulting from varying the atmospheric liquid water content.

Table 3. Surface Condition Determination

Channel Relationship	Surface Condition
$T_B(\nu_3) \leq .97 \, T_B(\nu_2)$	Dry Land
$1.01 \, T_B(\nu_2) \geq T_B(\nu_3) > .97 \, T_B(\nu_2)$	Wet Land
$T_B(\nu_3) > 1.01 \, T_B(\nu_2)$	Water, or Water-Land Combination

Using Table 3 to determine the appropriate surface condition, the linear regression equations for water vapor and liquid water over dry land surfaces are

$$Q = -65.17 + 22.90 \times 10^{-2} \, T_B(\nu_1) + 13.60 \times 10^{-3} \, T_B(\nu_2) \qquad (34a)$$

$$W = 18.52 \times 10^{-1} - 59.43 \times 10^{-4} \, T_B(\nu_1) - 39.00 \times 10^{-5} \, T_B(\nu_2) \qquad (34b)$$

The corresponding equations for wet land surfaces are

$$Q = 64.74 - 89.85 \times 10^{-2} \, T_B(\nu_1) + 68.05 \times 10^{-2} \, T_B(\nu_2) \qquad (35a)$$

$$W = 33.18 - 64.88 \times 10^{-2} \, T_B(\nu_1) + 53.36 \times 10^{-2} \, T_B(\nu_2) \qquad (35b)$$

The statistical results of these two sets of equations are summarized in Table 4.

Equations (34a) and (35a) enable the determination of water vapor over dry and wet land to within a standard error of 0.87 g cm^{-2} and 0.97 g cm^{-2}, respectively, while Eqs. (34b) and (35b) calculate liquid water content with standard errors of 0.18 kg m^{-2} and 0.22 kg m^{-2}. The effect of the statistical base on the results may be determined by the reduction in variance between the data and the regression

Table 4. SCAMS Regression Analysis

| Parameter (Equation) | Data Sample Statistics | | Regression Analysis Results | |
	Mean	Standard Deviation	Standard Error	Variance Reduction
Water Vapor over Dry Land (34a)	3.32 g cm^{-2}	1.75 g cm^{-2}	0.87 g cm^{-2}	75%
Liquid Water over Dry Land (34b)	0.27 kg m^{-2}	0.30 kg m^{-2}	0.18 kg m^{-2}	64%
Water Vapor over Wet Land (35a)	3.91 g cm^{-2}	1.93 g cm^{-2}	0.97 g cm^{-2}	74%
Liquid Water over Wet Land (35b)	0.38 kg m^{-2}	0.37 kg m^{-2}	0.22 kg m^{-2}	65%

equations. As has been previously reported (Grody, 1976 and Rosen-crantz, 1972), the percent reduction in variance is larger for water vapor than for liquid water, most importantly due to the effect of variations in cloud temperatures, which are not inferred from the satellite data. A total of 35 samples was used in each regression sample. To ensure the significance of the sample size, a larger sample was tested in each case, using 45 sample points. No further reduction in standard error resulted from this increase in sample size, verifying the statistical significance of the sample. Table 5 shows the regression coefficients and error analyses for two sample sizes.

   To provide an example of the use of these empirical formulas in the derivation of water vapor and liquid water content from SCAMS data, two days with significant weather were chosen and analyzed.

Table 5. Regression Coefficients and Error Analyses

Sample Size	Dependent Variate Y*	X_1*	X_2*	X_3*	Standard Error
35	Q (dry)	-65.17	22.90×10^{-2}	13.60×10^{-3}	.87 g cm^{-2}
45	Q (dry)	-64.72	23.40×10^{-2}	14.00×10^{-3}	.87 g cm^{-2}
35	W (dry)	18.52×10^{-1}	-59.43×10^{-4}	-39.00×10^{-5}	.18 kg m^{-2}
45	W (dry)	18.61×10^{-1}	-58.51×10^{-4}	-48.00×10^{-5}	.18 kg m^{-2}
35	Q (wet)	64.74	-89.85×10^{-2}	68.05×10^{-2}	.97 g cm^{-2}
45	Q (wet)	65.31	-89.53×10^{-2}	68.17×10^{-2}	.97 g cm^{-2}
35	W (wet)	33.18	-64.88×10^{-2}	53.36×10^{-2}	.22 kg m^{-2}
45	W (wet)	33.02	-62.93×10^{-2}	55.36×10^{-2}	.22 kg m^{-2}

* When equation is of the form $Y = X_1 + X_2 T_B(\nu_1) + X_3 T_B(\nu_2)$

5.2 Synoptic Discussion

The synoptic discussion for each of the two days includes a surface and 500 mb analysis at 1200Z and satellite data from NOAA 4. The two satellite pictures are the broad band visible (.5-.7 μm) channel and the broad band window (10.5-12.5 μm) channel, both at 1800Z.

August 22, 1975, 1200Z. The 500 mb analysis had a closed low at 58°N, 52°E with a trough line extending south-southwestward. A long wave trough line in the western United States was located through western Washington and Oregon, western Nevada, central California and out into the Pacific Ocean. The eastern United States was dominated by high pressure south of 40°N.

The surface map shows a low pressure center over eastern Maine, with an associated frontal system extending across southern Canada,
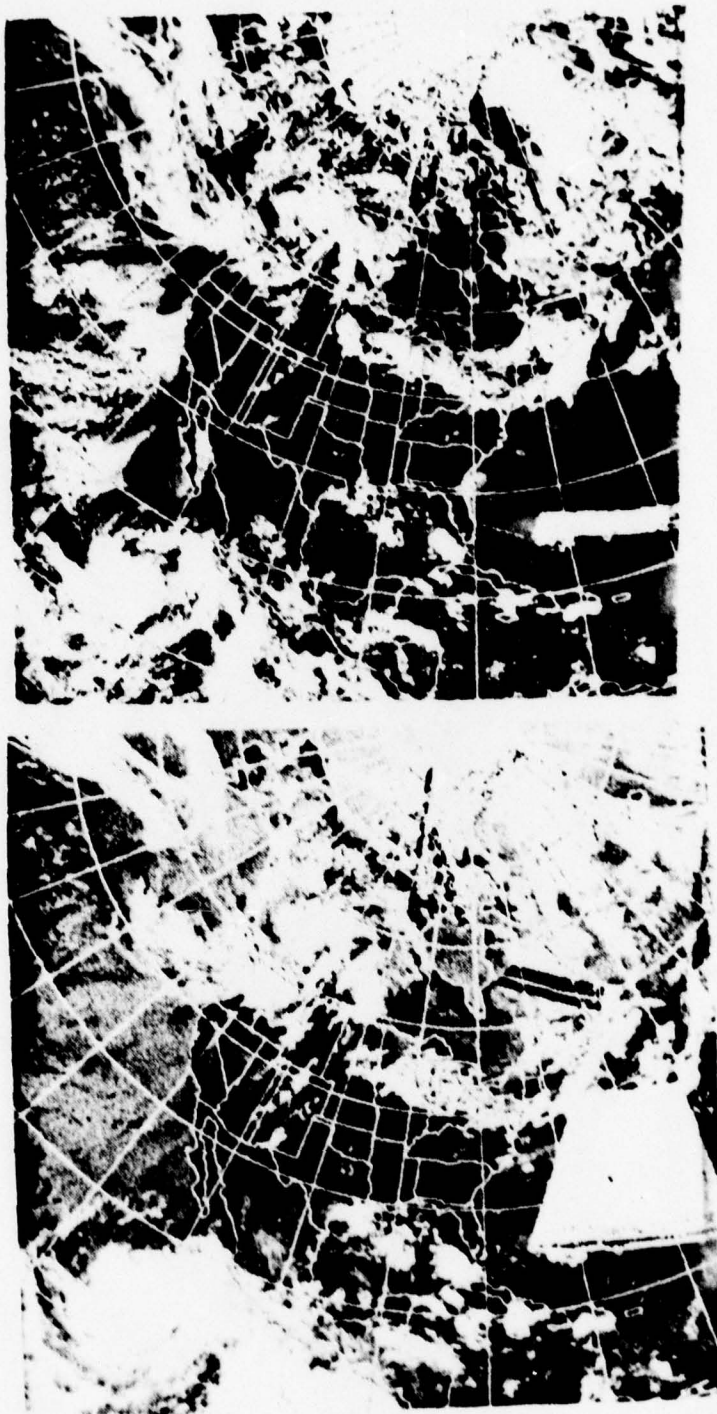
Figure 14. NOAA 4 mosaic for August 22, 1975 with the visible channel on the top and the infrared channel on the bottom.

southern Lake Michigan and across Iowa and Nebraska. Shower activity was present all along this frontal system. A low pressure area in Alberta had a cold front extending into Montana and Idaho, with a warm front through eastern Montana. Showers were present along this frontal system also.

The satellite pictures clearly reflect the frontal positions, with all the activity in the western United States north of 45^ON. The subtrack of the SCAMS pass was along a line from 18.7^ON, 91.6^OW to 52^ON, 104^OW. The pass had a time of 1745Z. Examination of the satellite pictures indicates a good cloud system north of 43^ON on the satellite subtrack.

August 25, 1975, 1200Z. The last day of the analysis had a closed low over central Canada, with a trough line extending southward through western Minnesota into Nebraska. A weak high was centered over southern California, while high pressure remained over the southeastern United States, weakening with the advancement of the trough.

A strong surface low was located southwest of Hudson Bay with a cold front extending through Lake Superior, south through Kansas and westward through Colorado. A stationary front extended across the Great Lakes and New York. Shower activity was present along the United States-Canada border from Maine to Montana, with heavy shower activity along the frontal system in Illinois, Iowa and Missouri. The satellite pictures reinforced the surface analyses with cloud cover in these areas. The SCAMS pass had a subtrack extending from 19^ON, 85.6^OW to 52^ON and 98.7^OW. This pass provided good coverage of the strong activity in the midwest as well as the clouds north of Lake
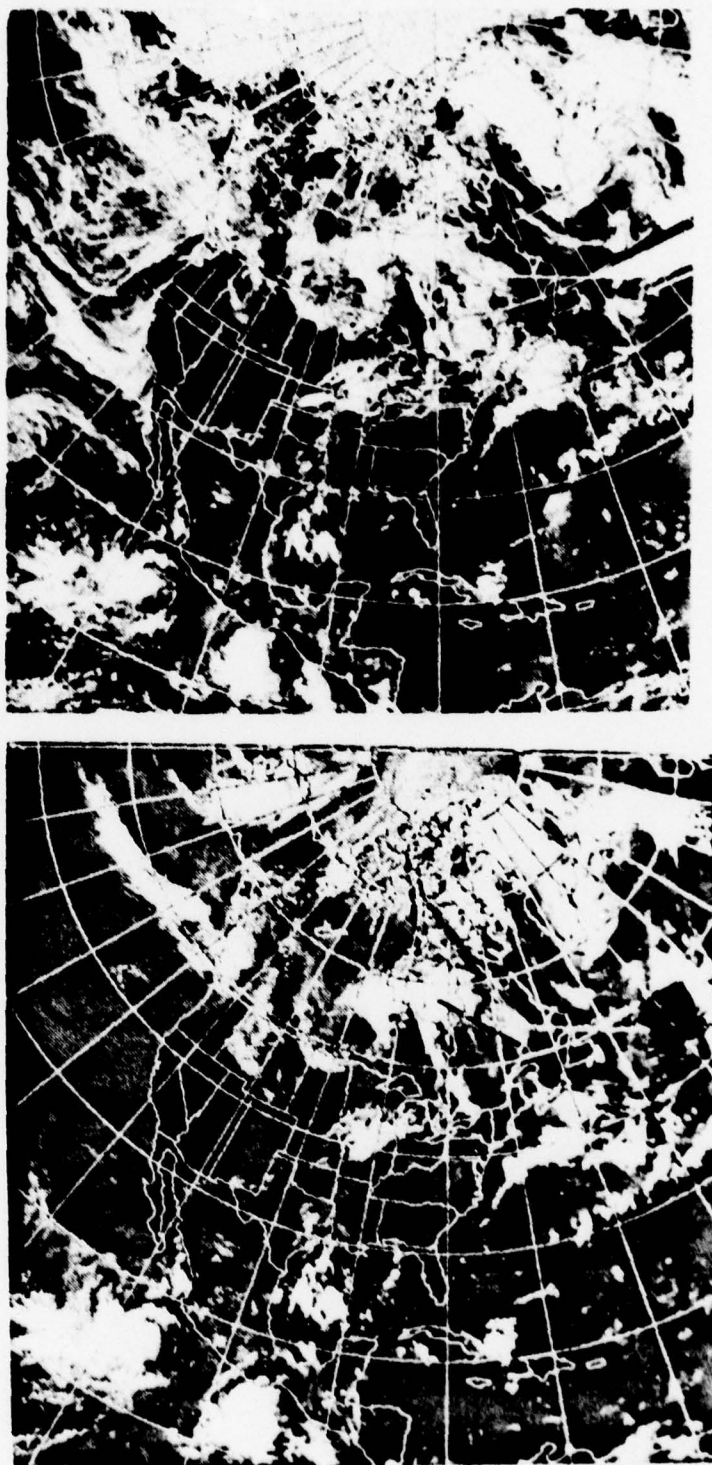
Figure 15. NOAA 4 mosaic for August 25, 1975 with the visible channel
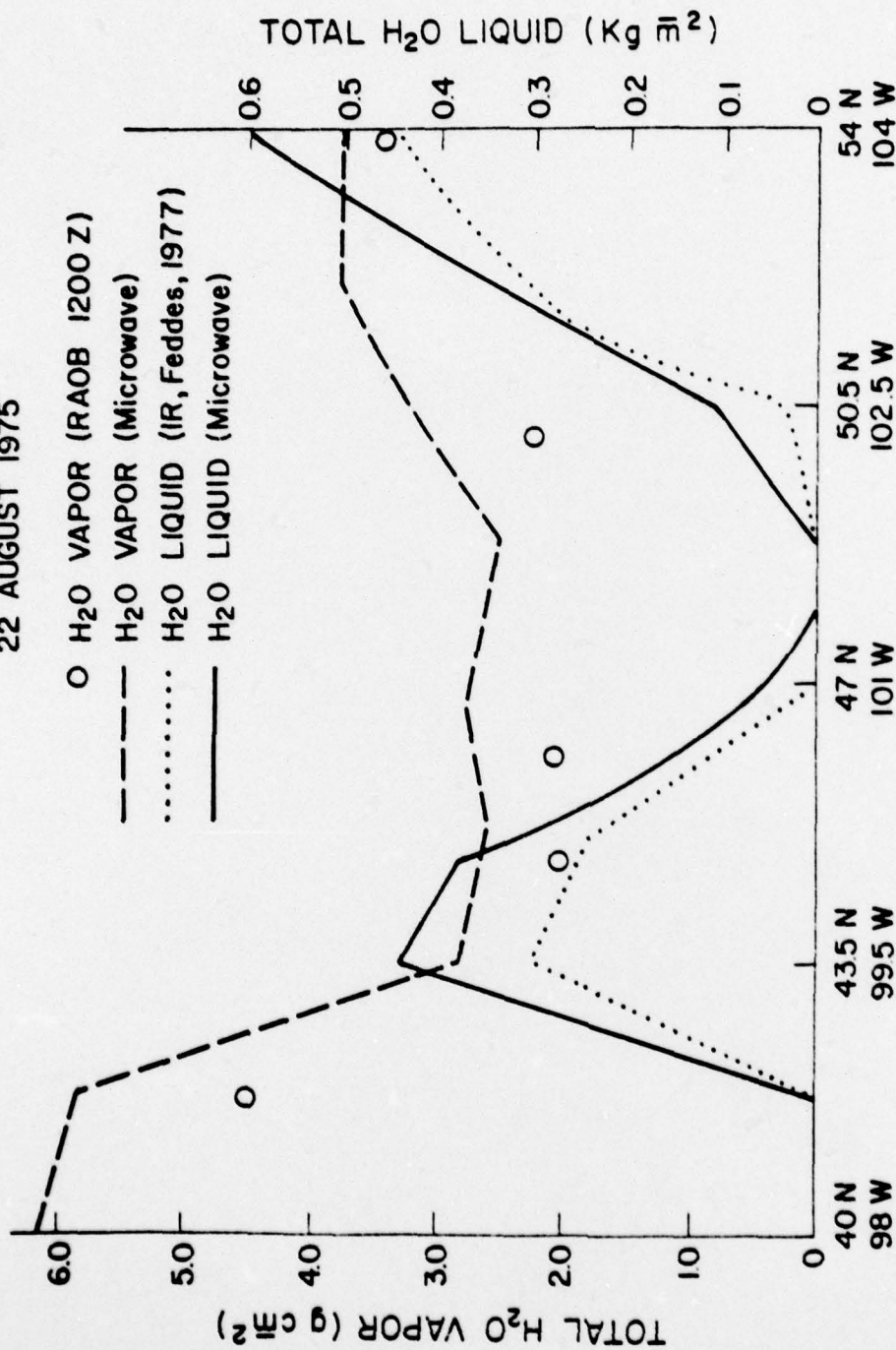on the top and the infrared channel on the bottom.

Superior.

5.3 Data Comparisons

The analysis of the SCAMS data for the two days is displayed in Figures 16-19. In Figures 16 and 17, the water vapor and liquid water values are plotted for the satellite subtrack for August 22 and August 25, respectively (see the IR pictures in Figures 14 and 15). The figures also contain radiosonde (RAOB) data where it was available within 300 km of the subtrack, and a plot of the liquid water derived by Feddes and Liou (1978) from HIRS data for the same subtrack and time frame. In general, wet surface conditions were found between 42^ON and 45^ON on August 22, while on August 25, the wet surface conditions were found between 40^ON and 42^ON and between 49^ON and 54^ON.

The water vapor estimates for both days generally correspond within 15 percent of the RAOB data, and appear to be biased larger than the RAOB data. The SCAMS data scan at satellite subtrack forms a circle approximately 144 km in diameter, providing data averaged over this area, while radiosonde data represent point measurements taken along the balloon flight trajectory, and thus may not be representative of the atmosphere as a whole. Instrument inaccuracy for the radiosonde water vapor measurements is estimated to be approximately 20 percent, thus contributing to the error. After further verification, microwave data could be used to verify and correct the RAOB data.

The SCAMS liquid water measurements may be compared to the satellite photographs and the results obtained from infrared data by Feddes and Liou. The analysis in Figure 16 for August 22 shows the effects

Figure 16. Calculated atmospheric water vapor and liquid water content compared to RAOB observations and results obtained by Feddes and Liou (1978) for August 22, 1975.
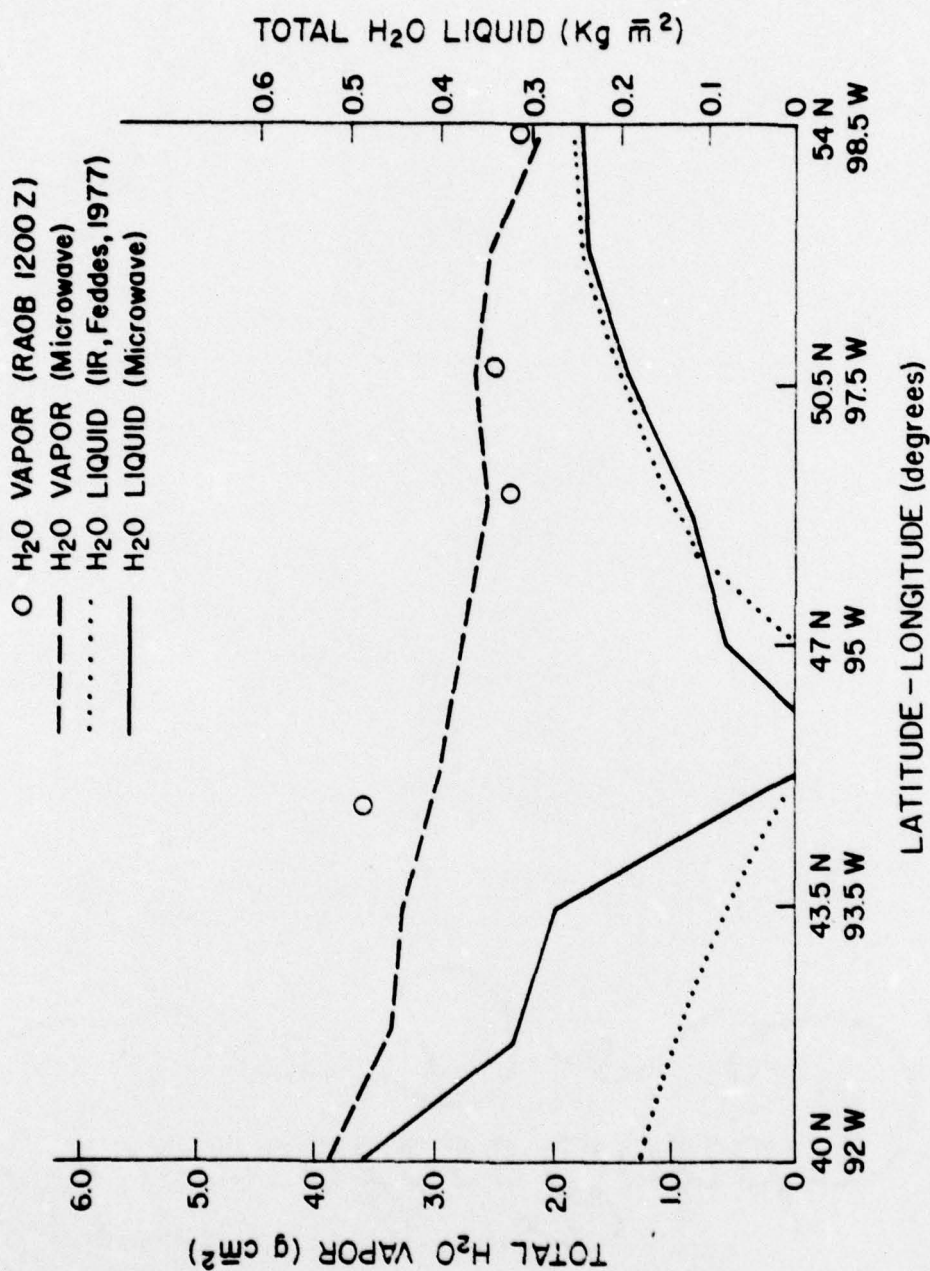
Figure 17. Calculated atmospheric water vapor and liquid water content compared to RAOB observations and results obtained by Feddes and Liou (1978) for August 25, 1975.

Figure 18.   Cloud liquid water content based on empirical-
theoretical calculations for August 22, 1975.
The isolines denote liquid water content (gm m⁻²).
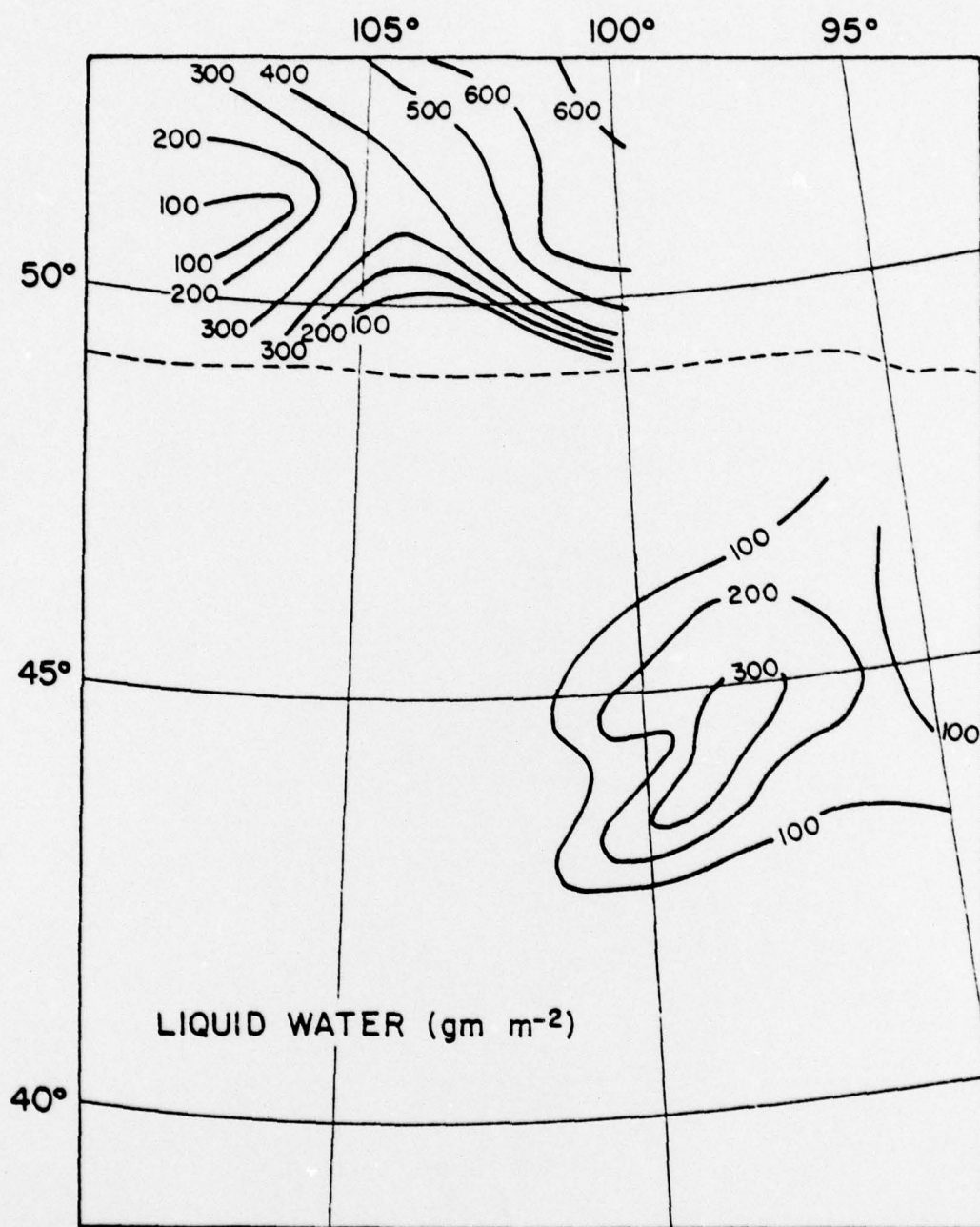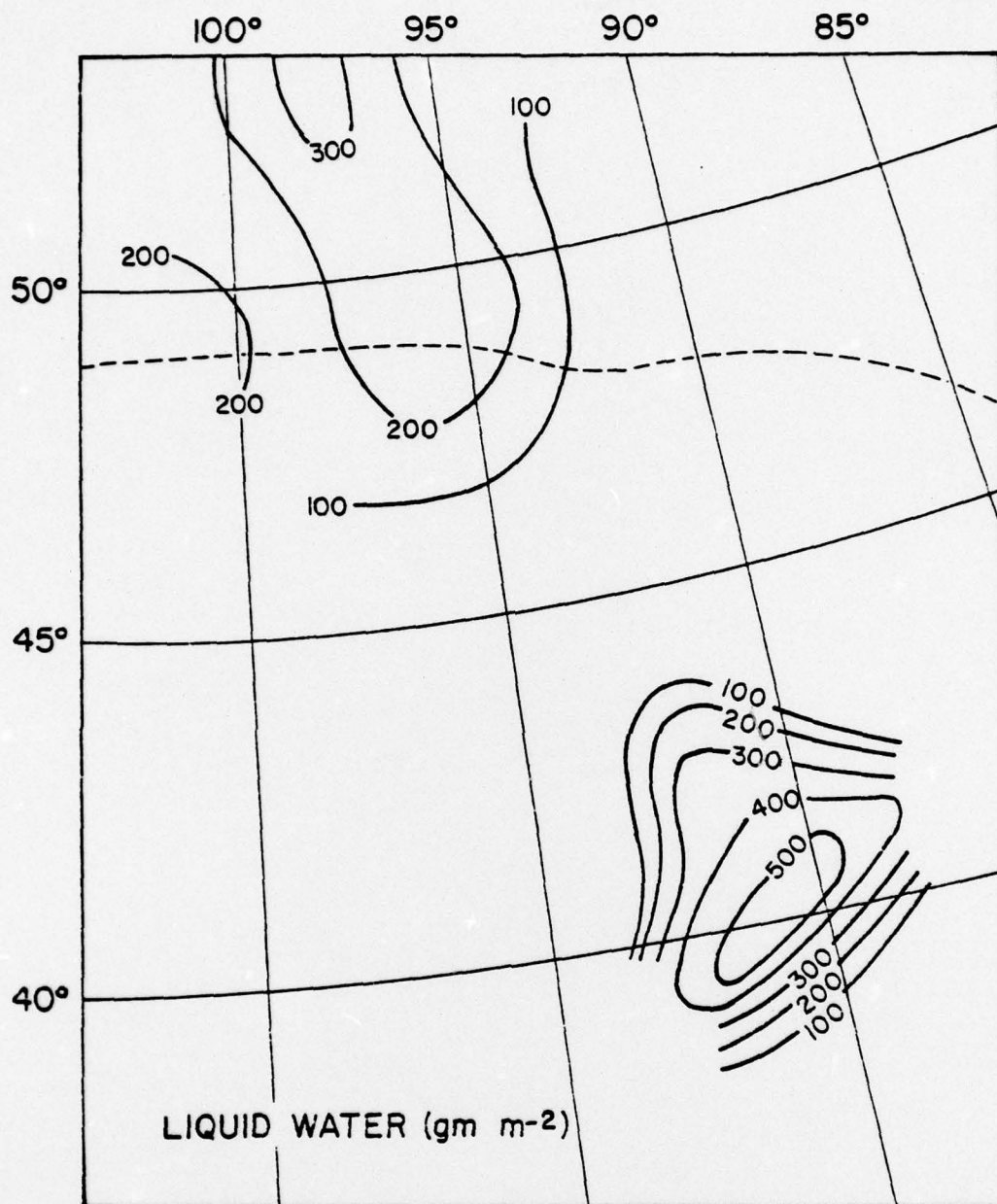
Figure 19. Cloud liquid water content based on empirical-
theoretical calculation for August 25, 1975.
The isolines denote liquid water content (gm m^{-2}).

of two overcast areas under the satellite pass. The Feddes results closely parallel the trend derived from the SCAMS data, but SCAMS data show higher liquid water contents in most cases. This is an expected result due to the capability of microwave to see through cloud layers, providing a better evaluation of lower cloud moisture levels. A similar result is shown in Figure 17. Again, two cloud masses are shown. The southern mass appears on the satellite photographs as an area of cirrus, and shows as an area of low water content in the Feddes study. The SCAMS data is not affected by the cirrus and yields for higher amounts of liquid water, revealing the area of active thunderstorms and rain under the cirrus clouds.

Figures 18 and 19 display the analyzed SCAMS liquid water content values plotted on a polar projection. The two figures contain the analysis for August 22 and August 25, respectively. The isolines are labeled with the liquid water content based on the theoretical calculations. Both figures show two distinct cloud masses. The analyses are quite similar to the results obtained by Feddes, with the modifications mentioned earlier. The smoothing effects of the larger scan results in only a minor loss of data compared with the results obtained by Feddes and Liou (1978). In Figure 18 of August 22, the two cloud areas correspond well with the satellite photographs of the same time, Figure 14. Analysis of Figure 19 also corresponds well to its matching satellite data, Figure 15. The line of thunderstorms in the southern cloud mass is hidden by the cirrus deck, but is well documented by the surface observations. The sharp southern edge of this cloud mass is well defined on the satellite photographs. The southern edge of the northern cloud mass also shows a sharp moisture gradient

which is evident on the surface weather depiction and satellite images.

Not plotted on Figures 18 and 19 are the rainfall rate results. For clarity, they will be presented here instead. For the two days studied, the observed rain cases under the satellite scans have a mean value of 1.56 mm per hour, with a standard deviation of 1.31 mm per hour. The theoretically calculated rainfall rates, based on the conversion of the liquid water content derivations for the same data points, have a mean value of 1.68 mm per hour, and a standard error of .68 mm per hour. This results in a 48% reduction of variance for this sample. Sources of error in this calculation would include the inherent inaccuracy in estimating precise point rain rates from calculated liquid water contents, as well as the errors induced by the large area covered by the SCAMS scan.

CHAPTER 6

CONCLUSIONS

A theoretical model to calculate the transfer of microwave radiation through cloudy and precipitating atmospheres was developed based on the discrete-ordinate method. Various cloud thicknesses, heights, and liquid water contents were used in this analysis. The model was adapted to the SCAMS channels of the Nimbus 6 satellite, and transmittances were obtained for each of the channels and used to generate upper and lower boundary conditions at the top and bottom of the cloud layer.

These calculations were then used by the transfer program to generate expected upwelling radiances over a range of satellite scan angles for each cloud configuration. After verification of these calculations with observed satellite radiances, the theoretical data were utilized to develop empirical formulas for the derivation of water vapor and liquid water content from the satellite data.

The theoretical parameterizations were applied to two days of SCAMS data and the results mapped and compared to visual and infrared satellite photographs, as well as to results obtained by Feddes and Liou (1978). The results compared favorably in both instances. The SCAMS data demonstrated a capability to sense liquid water hidden to infrared sensors by overlying cirrus layers, and to provide a smoothed map of atmospheric moisture for a variety of atmospheric conditions.

Before this technique could be applied on a global scale, several areas would require further study. The data base from which the samples were taken was limited to a two-week period in August, and the effects of certain surface conditions, such as snow cover, were not examined or considered. Extensive variations in surface elevation or temperature would also require adjustment of the empirical formulations. Another surface condition not addressed in this study is the case where the scan includes both a water surface and a land surface. This interface would occur near all significant bodies of water including large lakes, and large scale mapping accuracy would require investigation of this problem.

An important assumption made in this research, and in the research of Grody (1976), is the simplification that the transmittances are approximately unity below 40 GHz. This hypothesis was verified by calculations using the basic equations. In future research, it would be of interest to compare empirical formulas developed directly from the basic equations with the equations presented here. This research indicates that the increased accuracy would be negligible.

The use of this technique on a global scale would thus require these additional variables to be parameterized. It is likely that a large set of constants could be determined, with the proper constants determined for each point under consideration from point location and surface conditions. Ideally, as described by Feddes and Liou (1978), this technique would be used in conjunction with other sensors. Infrared sensors, such as the HIRS instrument aboard Nimbus 6, could provide better resolution than the microwave radiometers, and are capable of detecting cirrus clouds which are essentially transparent to the

microwave spectrum. In addition, infrared techniques might be more appropriate near water-land interfaces. The microwave technique is superior to the infrared for thicker clouds or multilayered clouds which are opaque to the infrared spectrum, and is less sensitive to water cloud temperature. The proper combination of infrared and micro-wave measurements can result in operationally significant data for moisture mapping. Using these sensors, global determination of total water content on a routine basis appears feasible.

REFERENCES

Born, M., and E. Wolf, 1975: Principles of Optics, 5th Edition. New York, Pergamon Press, 808 pp.

Chandrasekhar, S., 1950: Radiative Transfer. New York, Dover Publications, Inc., 393 pp.

Deirmendjian, D., 1969: Electromagnetic Scattering on Spherical Polydispersions. New York, Elsevier Publishing Co., 290 pp.

Edgerton, A., et al., 1971: Microwave emission characteristics of natural materials and the environment. Final Report No. 9016R-8 for Geography Branch, Earth Sciences Division, Office of Naval Research, Contract No. N00014-70C-0351, Aerojet-General Corporation, El Monte, California, 56 pp.

Feddes, R. G., and K. N. Liou, 1977: Cloud composition determination by satellite sensing using the Nimbus VI High Resolution Infrared Sounder. Scientific Report No. 3, Air Force Geophysics Laboratory, 199 pp.

_____, and _____, 1978: Atmospheric ice and water content derived from parameterization of Nimbus VI High Resolution Infrared Sounder data. J. Appl. Meteor., in press.

_____, and R. D. Smith, 1974: A synoptic scale model for simulating condensed atmospheric moisture. USAFETAC TN 74-4, United States Air Force Environmental Technical Applications Center, Washington, D. C., 31 pp.

Fryer, H. C., 1966: Experimental Statistics. Boston, Allyn and Bacon, Inc., 602 pp.

Gloersen, P., T. Wilheit, and T. Schmugge, 1972: Microwave emission measurements of sea surface roughness, soil moisture, and sea ice structure. Fourth Annual Earth Resources Program Review, NASA Programs, Goddard Space Flight Center, Greenbelt, Maryland, 8-19.

Goldstein, H., 1951: Attenuation by Condensed Water, Propagation of Short Radio Waves. New York, McGraw-Hill Book Co., Inc., 280 pp.

Grody, N. C., 1976: Remote sensing of atmospheric water content from satellites using microwave radiometry. IEEE Trans. on Antennas and Propagation, AP-24, 155-161.

Gunn, K. L. S., and T. W. R. East, 1954: The microwave properties of precipitation particles. Quart. J. Roy. Meteor. Soc., 80, 522-545.

_____, and J. S. Marshall, 1958: The distribution with size of aggregate snow flakes. J. Meteor., 15, 452-461.

Liebe, H. J., 1969: Molecular transfer characteristics of air between 40 and 140 GHz. IEEE Trans. on Microwave Theory and Techniques, MTT-23, 380-386.

Liou, K. N., 1973a: Transfer of solar irradiance through cirrus cloud layers. J. Geophys. Res., 78, 1409-1419.

_____, 1973b: A numerical experiment on Chandrasekhar's discrete-ordinate method for radiative transfer: Applications to cloudy and hazy atmospheres. J. Atmos. Sci., 30, 1303-1326.

_____, 1974a: On the radiative properties of cirrus in the window region and their influence on remote sensing of the atmosphere. J. Atmos. Sci., 31, 522-532.

_____, 1974b: Analytic two-stream and four-stream solutions for radiative transfer. J. Atmos. Sci., 31, 1473-1475.

_____, and J. E. Hansen, 1971: Intensity and polarization for single scattering by polydisperse spheres: A comparison of ray optics and Mie theory. J. Atmos. Sci., 28, 995-1004.

_____, and T. L. Stoffel, 1976: Remote sensing of cirrus cloud compositions. Scientific Report No. 1, AFGL-TR-0027, Air Force Geophysics Laboratory, 81 pp.

Marshall, J. S., and W. M. Palmer, 1948: The distribution of rain-drops with size. J. Meteor., 5, 165-166.

Meeks, M. L., and A. E. Lilley, 1963: The microwave spectrum of oxygen in the earth's atmosphere. J. Geophys. Res., 68, 1683-1703.

Rosencrantz, et al., 1972: Microwave radiometric measurements of atmospheric temperature and water from an aircraft. J. Geophys. Res., 77, 5833-5844.

Savage, R. C., 1976: The transfer of thermal microwaves through hydrometeors. Ph.D. dissertation, University of Wisconsin, Madison.

Schmugge, T., et al., 1974: Remote sensing of soil moisture with microwave radiometers. J. Geophys. Res., 79, 317-323.

Sekhon, R. S., and R. C. Srivastava, 1970: Snow size spectra and radar reflectivity. J. Atmos. Sci., 27, 299-307.

Staelin, D. H., et al., 1975: Microwave atmospheric temperature soundings: Effects of clouds on Nimbus V satellite data. J. Atmos. Sci., 32, 1970-1976.

————, et al., 1976: Remote sensing of atmospheric water vapor and liquid water with the Nimbus V microwave spectrometer. J. Appl. Meteor., 15, 1204-1214.

Stoffel, T. L., 1976: Radiative properties of cirrus clouds in the infrared: Applications to remote sensing. M.S. dissertation, University of Utah, Salt Lake City.

The Nimbus VI User's Guide, 1975, The Lansat/Nimbus Project, Goddard Space Flight Center, NASA, Greenbelt, Maryland, 227 pp.

VanVleck, J. H., 1974: The absorption of microwaves by oxygen. Phys. Rev., 71, 413-424.

Waters, J. W., et al., 1975: Remote sensing of atmospheric temperature profiles with Nimbus V microwave spectrometer. J. Atmos. Sci., 32, 1953-1969.

Wilheit, T. T., et al., 1977: A satellite technique for quantitatively mapping rainfall rates over the oceans. J. Appl. Meteor., 16, 551-560.

Wolfe, H. M., 1977: Clear column radiance program. Private communication.

VITA

Name	Alan Douglas Duff
Birthplace	Washington, D. C.
Birthdate	June 16, 1948
High School	DuVal Senior High School Glenn Dale, Maryland
Universities	West Virginia University Morgantown, West Virginia 1966-1970 Pennsylvania State University State College, Pennsylvania 1970-1971 University of Montana Missoula, Montana 1973-1976 University of Utah Salt Lake City, Utah 1976-1978
Degrees	B.S., 1970 West Virginia University Morgantown, West Virginia B.S., 1971 Pennsylvania State University State College, Pennsylvania M.B.A., 1976 University of Montana Missoula, Montana
Professional Position	Meteorologist, Captain Unites States Air Force